LAWRENCE
LIVERMORE
NATIONAL
LABORATORY

UCRL-JRNL-237116

Measurements of Molecular Mixing in a High Schmidt Number Rayleigh-Taylor Mixing Layer

N. J. Mueschke, O. Schilling, D. L. Youngs, M. Andrews

December 7, 2007

Journal of Fluid Mechanics

Disclaimer

UCRL-JRNL-237116

Measurements of Molecular Mixing in a High Schmidt Number Rayleigh–Taylor Mixing Layer

Nicholas J. Mueschke[1], Oleg Schilling[2], David L. Youngs[3] & Malcolm J. Andrews[4]

1) Department of Mechanical Engineering

Texas A&M University

College Station, TX 77843 USA

2) Lawrence Livermore National Laboratory

Livermore, CA 94551 USA

3) Atomic Weapons Establishment

Aldermaston, Reading, Berkshire RG7 4PR UK

4) Los Alamos National Laboratory

Los Alamos, NM 87545 USA

Submitted to: Journal of Fluid Mechanics

Date Submitted: December 10, 2007

Type of paper: Full-length article

Address of correspondence: Dr. Malcolm J. Andrews

Los Alamos National Laboratory

P.O. Box 1663

Mail Stop D413

Los Alamos, NM 87545

Tel: (505) 606-1430

Fax: (505) 665-4972

Email: mandrews@lanl.gov

Measurements of Molecular Mixing in a High Schmidt Number Rayleigh–Taylor Mixing Layer

Nicholas J. Mueschke, Oleg Schilling, David L. Youngs & Malcolm J. Andrews

Abstract

Molecular mixing measurements are performed for a high Schmidt number ($Sc \sim 10^3$), small Atwood number ($A \approx 7.5\times10^{-4}$) buoyancy-driven turbulent Rayleigh–Taylor mixing layer in a water channel facility. Salt was added to the top stream to create the desired density difference. The degree of molecular mixing was measured as a function of time by monitoring a diffusion-limited chemical reaction between the two fluid streams. The pH of each stream was modified by the addition of acid or alkali such that a local neutralization reaction occurred as the two fluids molecularly mixed. The progress of this neutralization reaction was tracked by the addition of phenolphthalein–a pH-sensitive chemical indicator–to the acidic stream. Accurately calibrated backlit optical techniques were used to measure the average concentration of the colored chemical indicator. Comparisons of chemical product formation for pre-transitional buoyancy- and shear-driven mixing layers are given. It is also shown that experiments performed at different equivalence ratios (acid/alkali concentration) can be combined to obtain a mathematical relationship between the colored product formed and the density variance. This relationship was used to obtain high-fidelity, quantitative measures of the degree of molecular mixing which are independent of probe resolution constraints. The dependence of such mixing parameters on the Schmidt and Reynolds numbers is examined by comparing the current $Sc \sim 10^3$ measurements with $Sc = 0.7$ gas-phase and $Pr = 7$ liquid-phase measurements. This comparison indicates that the Schmidt number has a large effect on the bulk quantity of mixed fluid at small Reynolds numbers $Re_h < 10^3$. At late times, all mixing parameters indicated a greater degree of molecular mixing and a decreased Schmidt number dependence. Implications for the development and quantitative assessment of turbulent transport and mixing models appropriate for Rayleigh–Taylor instability-induced mixing are discussed.

1. Introduction

A fundamental understanding of the physics of turbulence is crucial to the development of predictive models of turbulent mixing. Historically, shear-driven turbulence, passive scalar mixing, and combustion have received extensive experimental, numerical, and theoretical attention (Warhaft 2000; Veynante & Vervisch 2002; Fox 2003; Dimotakis 2005). Mixing induced by buoyancy-driven turbulence remains an open area of research, as such flows become complex due to the coupling of the density field with the velocity field. The present study uses a novel combination of passive scalar and reacting flow experimental techniques to investigate molecular mixing dynamics in a high Schmidt number, Rayleigh–Taylor instability-driven turbulent mixing layer.

1.1 *Overview of the Rayleigh–Taylor instability*

The Rayleigh–Taylor instability occurs when a heavier fluid of density ρ_1 is accelerated into a lighter fluid of density ρ_2, typically by gravity (Rayleigh 1884; Taylor 1950). At early times, when the amplitudes of the initial perturbation at the interface between the two fluids are much smaller than their respective wavelengths, such perturbations grow according to linear instability theory (Chandrasekhar 1961). The structures of rising lighter fluid are referred to as "bubbles", and the structures of falling heavier fluid are referred to as "spikes". As the amplitudes of the growing bubbles and spikes approach the perturbation wavelength, the mixing layer transitions into a nonlinear growth phase (Youngs 1984; Haan 1989). The flow eventually becomes turbulent and grows self-similarly. In the small Atwood number case considered here, the fronts of the penetrating bubbles and spikes ($h_b \approx h_s \approx h/2$) grow nearly symmetrical and the total width of the mixing layer h grows as (Anuchina 1978; Youngs 1984):

$$\frac{h}{2} = \alpha A g t^2 , \tag{1.1}$$

where the Atwood number $A = \left(\rho_1 - \rho_2\right)/\left(\rho_1 + \rho_2\right)$ is a dimensionless measure of the density contrast between the fluids, g is the acceleration, and α is a dimensionless growth parameter.

Rayleigh–Taylor instabilities occur in a variety of physical processes, and over a wide

range of length- and time-scales. Buoyancy-driven hydrodynamic instabilities, including the Rayleigh–Taylor instability, may limit the formation of heavy elements during stellar implosions (Smarr *et al.* 1981). On a smaller scale, many oceanographic and atmospheric currents are buoyancy-driven due to temperature or concentration gradients (Molchanov 2004; Cui & Street 2004). On a yet smaller scale, the breakup of fuel droplets in internal combustion engines has been related to Rayleigh–Taylor instabilities (Thomas 2003; Marmottant & Villermaux 2004). At very small scales, the implosion of inertial confinement fusion (ICF) target capsules are highly susceptible to acceleration-driven instabilities, where mixing of the hot inner fuel and the cold outer shell material can limit the total energy yield (Lindl 1998; Betti *et al.* 2001; Atzeni & Meyer-ter-Vehn 2004). Buoyancy-generated turbulence provides an efficient mechanism for mixing the constituent miscible fluids (Linden & Redondo 1991). Despite the importance that molecular mixing may have in these applications, a comprehensive understanding of the buoyancy-driven mixing process, the coupled molecular mixing, and the associated modeling remain largely unexplored.

1.2 *Previous measurements of molecular mixing*

Quantitative measurements of molecular mixing have been reported for many classical, shear-driven turbulent flows. In particular, a variety of experiments have been designed to monitor a diffusion-limited chemical reaction to quantify the degree of molecular mixing. Konrad (1977) examined gas-phase mixing in free-shear flows with an associated Schmidt number of $Sc = \nu/D = 0.7$ (ν is the kinematic viscosity and D is the species diffusivity). Breidenthal (1979, 1981) performed similar measurements in liquid-phase turbulent shear layers with $Sc \sim 10^3$. Both Konrad and Breidenthal quantified the degree of molecular mixing using backlit optical techniques to measure the absorption of light by a specific chemical species. A key result from these studies was an integral measure of the chemical product concentration, P/δ, where P is the equivalent thickness of chemical product across the mixing layer, and δ is the width (vorticity thickness) of the turbulent shear layer. It was reported that P/δ is a function of the Schmidt number, velocity ratio $r = U_1/U_2$, initial conditions, and Reynolds number up to a

transition range after which the mixing layer became entrainment-limited. Once the mixing layer crossed the threshold Reynolds number range, P/δ became independent of all parameters except the Schmidt number. For Sc = 0.7 experiments, Konrad (1977) reported $P/h \approx 0.65$ for $Re_\delta = \Delta U\,\delta/\nu < 5000$, and $P/\delta \approx 0.81$ at higher Reynolds numbers. This contrasts with the much lower values reported for the liquid-phase experiments (Breidenthal 1979, 1981), where $P/\delta = 0.05\text{–}0.3$ was measured in pre-transitional mixing layers at different velocity ratios, and $P/\delta = 0.365 \pm 0.02$ at $Re_\delta > 8000$. Koochesfahani and Dimotakis (1986) extended this work by using a combination of passive scalar and reacting flow techniques to quantify the amount of chemical product formed (measuring post-transition values of P/δ) and the probability density function (PDF) of the high-speed fluid. The statistical composition of the mixed fluid was quantified by calculating the first moment of the interior portion of the high-speed fluid PDF. Combining all of these results, the scalar Schmidt number of the flow was found to have a significant influence on the degree of molecular mixing both before and after the mixing transition in shear flows.

Reacting flow techniques have also been used to measure mixing in turbulent jets. Shea (1977) used chemically-reacting gases to measure the effects of the Reynolds number and equivalence ratio on the reduction of the initial chemical reactants. Zhang *et al.* (1995) and Zhang & Schneider (1995) used a similar liquid-phase configuration, phenolphthalein indicator, and experimental methods as Breidenthal used (1979, 1981) to study how variations in exit geometry affected the degree of molecular mixing in turbulent jets. Analogous to the measurement of P/δ by Konrad (1977) and Breidenthal (1979, 1981), Zhang *et al.* (1995) also quantified the degree of molecular mixing by integrating the measured concentration chemical indicator across the span of the jet at specific downstream locations. It was concluded that the total amount of chemical product formed can be increased by modifying the jet exit geometry.

Few such measurements of molecular mixing have been reported for turbulent Rayleigh–Taylor driven mixing layers. Using a water channel (Wilson & Andrews 2002; Ramaprabhu & Andrews 2004; Mueschke *et al.* 2006) analogous to the two-stream configurations used by

Konrad (1977) and Breidenthal (1979, 1981), the degree of molecular mixing was measured for a buoyancy-driven mixing layer, where one stream was heated so that $T_1 \neq T_2$. A complete description of the water channel facility is provided in § 2. In this configuration, temperature was a marker for the density and $Pr = \nu/\chi \equiv Sc = 7$, where χ is the thermal diffusivity of water. No chemical reaction was used in these experiments, instead a high resolution thermocouple system measured pointwise temperatures that were then related to density through an equation of state (Kukulka 1981). Mueschke *et al.* (2006) reported the time-evolution of the molecular mixing parameter θ, defined in (4.4) and analogous to the intensity of segregation parameter (Dankwerts 1950), along the centerplane of the mixing layer. Banerjee *et al.* (2007) used hot-wire techniques to measure late-time values of θ in analogous gas-phase experiments using air and helium, in which $Sc = 0.7$.

The water and gas channel experiments just described reported measurements for moderate species diffusivities cases of $Sc = 0.7$ and $Sc = 7$. A different set of experiments by Linden and Redondo (1991) and Linden *et al.* (1994) considered the degree of molecular mixing in a Rayleigh–Taylor mixing layer, in which the density difference was created by adding salt to the top fluid, such that $Sc \sim 10^3$. In these experiments, an unstable stratification of salt water over fresh water was created when a thin barrier separating the fluids was quickly removed. Linden *et al.* (1994) used two separate measurement techniques to quantify the degree of mixing. First, electrical conductivity probes were used to measure the salt concentration pointwise. In addition, methods similar to those used by Breidenthal (1979) and Zhang *et al.* (1995) were adopted to measure the formation of colored phenolphthalein indicator. However, the resulting product formation measurements were limited to the concentration profiles of the indicator for a single equivalence ratio [see (3.3)], and the time-evolution of the centerplane indicator concentration at several equivalence ratios. The present work will also report profiles of chemical product formation; however, these results will be extended by developing a relationship between the measured product concentrations and a molecular mixing parameter θ, and its global equivalent Θ, both defined in § 4.

1.3 *Present investigation*

The current work combines aspects of the reacting flow experiments of Breidenthal (1979; 1981), Zhang *et al.* (1995), and Linden *et al.* (1994) with a water channel used to investigate Rayleigh–Taylor driven turbulent mixing. Novel experimental techniques were developed, combining passive scalar measurements and reacting flow measurements at various equivalence ratios to obtain resolution-independent measurements of both mean and fluctuating density statistics. These results were used to calculate various parameters which quantify the degree of molecular mixing. This paper is organized as follows. First, an overview of the water channel facility, indicator chemistry, and optical diagnostics is presented. Measurements of the colored chemical product formation are then presented, and the results are compared with the $Sc \sim 10^3$ shear-driven mixing results of Breidenthal (1979, 1981) for validation purposes. The chemical product measurements are used to obtain the first resolution-independent measurements for the $Sc \sim 10^3$ case of several commonly used parameters that quantify the degree of molecular mixing. A relationship between the chemical product formed and the density variance is developed, and the measurements are presented. Comparisons of the molecular mixing parameter θ are given for the $Sc = 0.7$ (Banerjee *et al.* 2007), $Pr \equiv Sc = 7$ (Mueschke *et al.* 2006), and $Sc \sim 10^3$ cases, and the results are discussed. Finally, the implications of these measurements for the development, calibration, and assessment of turbulent transport and mixing models are discussed.

2. Experimental facility

Experiments were performed using an open loop water channel facility (Snider & Andrews 1994; Wilson & Andrews 2002; Ramaprabhu & Andrews 2004; Mueschke *et al.* 2006) supplied by two 500 gallon water tanks (see figure 1). Two streams of water were pumped into the channel and separated by a thin splitter plate. A series of flow straighteners and wire meshes mitigated free-stream turbulence and boundary layers (Koop 1976; Browand & Weidman 1976; Stillinger *et al.* 1983). An unstable stratification of a heavier fluid over a lighter fluid developed

downstream of the splitter plate, which transitioned to a turbulent mixing layer as the heavier fluid fell and the lighter fluid rose. The layer was advected downstream by a mean velocity $U_m \approx 5$ cm/s, and the time-evolution of the mixing layer was related to downstream distance by Taylor's hypothesis $t = x/U_m$ (Pope 2000). Time was normalized as

$$\tau = t\sqrt{\frac{A\,g}{H}}\,, \tag{2.1}$$

where $H = 32$ cm is the vertical height of the channel. The water channel provides a unique facility for measuring turbulence statistics, as the mixing layer is statistically-stationary and long sampling times are available.

In the set of experiments presented here, salt (NaCl) was added to the top stream of the channel to create a density difference. In this case, the concentration of salt served as a marker for the density field. The resulting species diffusivity of the Na^+ and Cl^- ions gave a Schmidt number $Sc = 620$ (Lide 2006). Direct measurements of the salt concentration field were not feasible due to the large magnitudes of the scalar gradients (Mueschke & Andrews 2005). Instead, a diffusion-limited chemical reaction between the two streams was monitored to measure the degree of molecular mixing. The pH of each stream was altered by adding either hydrochloric acid (HCl) or sodium hydroxide (NaOH) to each stream. As the two fluids mixed at the molecular level, a neutralization reaction occurred and the local pH of the mixture reached a new equilibrium. The reaction was monitored by the addition of a pH-sensitive chemical indicator (phenolphthalein) to the acidic stream. As the local pH of the mixture changed, the transparent phenolphthalein changed color to a translucent shade of pink. The concentration of the colored form of the indicator was measured using backlit optical techniques. This section presents an overview of the prerequisite chemistry, optical measurement techniques, and estimated measurement uncertainty bounds.

2.1 *Reaction chemistry*

In the current experiments, fluid 1 is the heavier fluid with $pH_1 > 7$ (alkali) and fluid 2 is the lighter fluid with $pH_2 \leq 7$ (either acidic or neutral), where the subscript denotes either the top

(heavy) or bottom (light) stream. In aqueous solutions, the concentration of hydrogen and hydroxide ions remains balanced according to the reversible reaction

$$\mathrm{H_2O} \rightleftharpoons \mathrm{H^+ + OH^-} \tag{2.2}$$

with associated equilibrium constant

$$K_w = [\mathrm{H^+}][\mathrm{OH^-}] = 1\times10^{-14}, \tag{2.3}$$

where square brackets $[\bullet]$ denote molar concentration, *i.e.* moles per liter (Harris 2003). As fluid from each stream molecularly mix, the local concentrations of H^+ and OH^- adjust to a new equilibrium value satisfying (2.3). The pH of the resulting mixture is $\mathrm{pH}_{mix} = -\log_{10}[\mathrm{H^+}]_{mix}$. Further details on the neutralization reaction are given in Appendix A.

In this work, the pH is controlled by the addition of HCl or NaOH to either stream. Given stoichiometric quantities of HCl and NaOH, *i.e.* both reactants are completely consumed in the reaction, the resulting mixtures will react according to the exothermic reaction $\mathrm{HCl}(aq) + \mathrm{NaOH}(aq) \longrightarrow \mathrm{H_2O}(l) + \mathrm{NaCl}(aq)$ with heat release $\Delta h_f^0 = -59.8$ kJ/mol. Given a specific heat capacity of water $C_p = 4.179$ J/g-K, the local temperature increase in the fluid is $\Delta T \approx 0.02°$ C for the case of $\mathrm{pH_1} = 11.5$ and $\mathrm{pH_2} = 2.5$. Accordingly, the local decrease in density due to thermal expansion is negligible and thus, the neutralization reaction has a negligible effect on the Atwood number or on the buoyancy effects driving the mixing.

To monitor the neutralization reaction, a small quantity of phenolphthalein ($C_{20}H_{14}O_4$) indicator was dissolved in the bottom (acidic) stream; the notation In is used to denote the indicator. Typical concentrations of $[\mathrm{In}]_2 = 6\times10^{-6}$ M were used, where the subscript indicates that the indicator was added to the bottom stream. While the chemistry of the neutralization reaction is straightforward, the chemistry of the pH-sensitive indicator is complex. Phenolphthalein is a weak acid, and will dissociate depending upon the local pH (Bishop 1972). Schematically, the indicator follows the reversible reaction

$$\text{Transparent Indicator} + 2\mathrm{OH^-} \rightleftharpoons \text{Colored Indicator}. \tag{2.4}$$

Phenolphthalein has multiple ionization states and, thus, several different chemical forms

(denoted by Roman numeral subscripts):

$$\mathrm{In_I} \rightleftharpoons \mathrm{In_{III}} + \mathrm{H^+}, \tag{2.5}$$

$$\mathrm{In_{III}} \rightleftharpoons \mathrm{In_{IV}} + \mathrm{H^+}, \tag{2.6}$$

$$\mathrm{In_{III}} \rightleftharpoons \mathrm{In_{VII}} + 2\mathrm{H^+}. \tag{2.7}$$

All forms of the indicator in (2.5)–(2.7) are transparent with the exception of the pink quinone phenolate form ($\mathrm{In_{IV}}$). The equilibrium constants for the first two reactions are (Kolthoff 1937)

$$K_1 = \frac{[\mathrm{In_{III}}][\mathrm{H^+}]}{[\mathrm{In_I}]} = 1.15\times10^{-9}, \tag{2.8}$$

$$K_2 = \frac{[\mathrm{In_{IV}}][\mathrm{H^+}]}{[\mathrm{In_{III}}]} = 2.8\times10^{-10}. \tag{2.9}$$

As the pH of a mixture rises above pH = 8, the equilibria of (2.5) and (2.6) move to the right according to Le Chatelier's principle, and the colored form of the indicator is produced. However, as pH > 11.3, the equilibrium of the reaction in (2.7) also moves to the right and, as a result, less $\mathrm{In_{III}}$ is available for the reaction in (2.6) and less colored indicator $\mathrm{In_{IV}}$ is formed. Zhang *et al.* (1995) reported a measurement of the equilibrium constant

$$K_3 = \frac{[\mathrm{In_{VII}}][\mathrm{H^+}]^2}{[\mathrm{In_{III}}]} \approx 2.75\times10^{-23} \tag{2.10}$$

for this reaction. An expression for the fraction of indicator in its colored form can be obtained by substituting the equilibrium constant expressions (2.8)–(2.10) into the mass balance equation

$$[\mathrm{In}] = [\mathrm{In_I}] + [\mathrm{In_{III}}] + [\mathrm{In_{IV}}] + [\mathrm{In_{VII}}]. \tag{2.11}$$

Solving for $[\mathrm{In_{IV}}]/[\mathrm{In}]$ gives a relative measure of concentration of $\mathrm{In_{IV}}$ as a function of the $\mathrm{H^+}$ concentration (Harris 2003). The fraction of dissociation of $\mathrm{In_{IV}}$,

$$\alpha_{\mathrm{In_{IV}}} = \frac{[\mathrm{In_{IV}}]}{[\mathrm{In}]} = \frac{K_1 K_2}{K_1 K_2 + K_1[\mathrm{H^+}] + [\mathrm{H^+}]^2 + K_1 K_3 [\mathrm{H^+}]^{-1}}, \tag{2.12}$$

is defined such that $\alpha_{\mathrm{In_{IV}}} = 0$ when none of the indicator is in its colored form, and $\alpha_{\mathrm{In_{IV}}} = 1$ when all of the indicator is in its colored form. Figure 2 shows the fraction of dissociation $\alpha_{\mathrm{In_{IV}}}$ as a function of the pH.

2.2 *Optical imaging system and calibration*

All constituents of the mixing layer and forms of the chemical indicator are transparent except for the final product $\mathrm{In_{IV}}$, which absorbs green light (λ_{peak} = 552 nm), and is therefore pink (Green 1990). The attenuation of a light ray passing through the mixing layer is related to the concentration of colored indicator $[\mathrm{In_{IV}}]$ through the Beer–Lambert law (Hecht 2002)

$$\sigma = \varepsilon \int_0^L [\mathrm{In_{IV}}]\,\mathrm{d}x, \tag{2.13}$$

where σ is the absorption of light, ε is a molar absorptivity constant for phenolphthalein, and L is the total path-length of the light ray through the absorbing medium. The absorption of light is related to the ratio of measured light intensity I to the backlighting intensity I_0 by

$$\sigma = -\ln\left(\frac{I}{I_0}\right) = \varepsilon L\overline{[\mathrm{In_{IV}}]}, \tag{2.14}$$

where $\overline{[\mathrm{In_{IV}}]}$ is the spanwise average concentration of colored indicator. Thus, given a calibrated value of the molar absorptivity ε, $\overline{[\mathrm{In_{IV}}]}$ is linearly related to a light absorption measurement. Colored indicator concentration measurements normalized by the free stream indicator concentration $C = \overline{[\mathrm{In_{IV}}]}/[\mathrm{In}]_2$ are presented in § 3.2.

In the present work, the molar absorptivity coefficient of phenolphthalein was measured by filling a Plexiglas wedge with a known concentration of indicator at a specified pH. The variation in light absorption across the wedge provided a measure of the light absorption versus depth of the wedge. The molar absorptivity coefficient was measured by calculating the slope of the absorption curve shown in figure 3. The calibration experiment was repeated using three different indicator concentrations: each produced similar slopes such that $\varepsilon_{\mathrm{In}} = 2.935\times10^4 \pm 0.67\%$ $(\mathrm{M\cdot cm})^{-1}$, which agreed well with the value $\varepsilon_{\mathrm{In}} = 2.934\times10^4$ $(\mathrm{M\cdot cm})^{-1}$ measured by Zhang *et al.* (1995). It was found that at absorptions $\sigma > 1.5$ the system response became nonlinear, so the phenolphthalein concentration in the acidic stream was limited to exclude absorptions $\sigma > 1.2$.

To measure the concentration of the colored form of phenolphthalein in the channel, the

experiment was backlit by multiple fluorescent lights. Prismatic panels and sheets of translucent velum were placed between the light source and the mixing section of the channel to create a uniform backlighting source. Attenuation of the background lighting by the colored phenolphthalein indicator was measured using an 8-bit, three-channel CCD array. A green optical filter was used to minimize the transmission of wavelengths above and below the peak absorption wavelength of phenolphthalein to the CCD array. Approximately two hundred photographs were used to measure the average light absorption by the indicator, and thus, through the Beer–Lambert law (2.14), the average concentration of $\overline{[\mathrm{In}_{\mathrm{IV}}]}$ at downstream locations.

2.3 *Uncertainty analysis*

The density difference between the two fluids was created by adding salt to the top stream. The density of each fluid was obtained by measuring the mass of a 50 ml sample in a high-accuracy flask on an electronic balance. Multiple samples were measured ($N \approx 8$–10) and the density of each fluid stream $\rho_r = m_r/V$ (where $r = 1,2$ denotes the top and bottom streams) was determined. The 95% confidence interval bounds were obtained from

$$w_{m_r} = \pm 1.96\sqrt{\frac{s_{m_r}^2}{N}}\,, \tag{2.15}$$

where $s_{m_r}^2$ is the variance of the mass measurements, and N is the number of samples (Benedict & Gould 1996). The resulting uncertainty in the density of each fluid is

$$w_{\rho_r} = \pm\sqrt{\left(\frac{\partial \rho_r}{\partial m_r} w_{m_r}\right)^2 + \left(\frac{\partial \rho_r}{\partial V} w_V\right)^2}\,, \tag{2.16}$$

where $w_V = \pm 0.05$ ml is the uncertainty in the volume measurement. Similarly, the uncertainty in the Atwood number for a given experiment is

$$w_A = \pm\sqrt{\left(\frac{\partial A}{\partial \rho_1} w_{\rho_1}\right)^2 + \left(\frac{\partial A}{\partial \rho_2} w_{\rho_2}\right)^2} = \pm 1\%\,. \tag{2.17}$$

The velocity of each stream was measured by injecting dye into the top and bottom streams, and recording the time required for the dye to travel a measured distance. Using similar uncertainty

propagation estimates as in (2.16) and (2.17), the mean advection velocity of the two streams was known to within ±2%. The uncertainty in the mean advection velocity was the greatest contributor to the uncertainty of the dimensionless time τ [see (2.1)], which was also known to within ±2%.

Uncertainties in the mean colored indicator concentration measurements were due to several sources, including the uncertainty in the free stream concentration of the indicator $w_{[\mathrm{In}]_2}$, the molar absorptivity coefficient w_ε, the light absorption measurement w_σ, and the width of the channel w_{L_y}. Furthermore, uncertainty in the phenolphthalein concentration in the bottom stream was determined by uncertainties in the volume of phenolphthalein added (±5 ml) and the volume of water in the bottom stream tank (1890 ± 2% liters). Taken together, this gives a relative uncertainty in the concentration of chemical indicator in the bottom stream of ±1.4%. The molar absorptivity coefficient from the calibration experiments in § 2.3 was determined to have an uncertainty of ±0.67%. Finally, uncertainty in the light absorption measurements were due to variations in the background lighting intensity and statistical uncertainty in the estimation of the mean light intensity measured from an ensemble average of ~ 200 images. The root-mean-square amplitude of the background lighting fluctuations was 0.8 intensity units on a scale from 0–255 from the 8-bit CCD. Accordingly, the intensity of the background lighting was steady to within ±0.5%. Combining all of these uncertainties gives an uncertainty of the measured chemical concentration *C* of

$$w_C = \pm\sqrt{\left(\frac{\partial C}{\partial \sigma} w_\sigma\right)^2 + \left(\frac{\partial C}{\partial \varepsilon} w_\varepsilon\right)^2 + \left(\frac{\partial C}{\partial L_y} w_{L_y}\right)^2 + \left(\frac{\partial C}{\partial [\mathrm{In}]_2} w_{[\mathrm{In}]_2}\right)^2} = \pm 3\% . \qquad (2.18)$$

3. Passive scalar and chemical indicator measurements

3.1 *Measurement of mixing layer growth*

As an initial check of the experimental facility and diagnostics, the mixing layer width was measured for the salt/fresh water configuration. Nigrosine dye (5 g) was added to the tank

supplying the top stream and the absorption of light was measured using the techniques discussed in § 2.2. A sample image from an experiment using the inert dye is shown in figure 4. The dye absorptivity coefficient was measured using the same Plexiglas wedge and light absorption techniques discussed in § 2.2. Experiments using the dye were then performed and the absorption of the backlighting was related to the mean dye concentration. The mean dye concentration was normalized by the free stream dye concentration and related to the mean heavy fluid (top stream) volume fraction by

$$\overline{f}_1 = \frac{\overline{\rho} - \rho_2}{\rho_1 - \rho_2} = \frac{\overline{[Dye]}}{[Dye]_1}, \tag{3.1}$$

where $\overline{f}_1$ is a dimensionless measure of the mean density field. Profiles of $\overline{f}_1$ at several downstream locations are shown in figure 5. As expected for small Atwood number Rayleigh–Taylor mixing layers (Youngs 1984; Snider & Andrews 1994), the growth of the mixing layer is symmetric about $\overline{f}_1 = 0.5$ with approximately linear profiles. The mixing layer width was determined by identifying the 5–95% thresholds from the $\overline{f}_1$ profiles. The growth parameter α = 0.085 ± 0.005 was obtained by measuring the slope of the half-width of the mixing layer plotted against Agt^2, as shown in figure 6. Ristorcelli and Clark (2004) showed that a measurement of α directly from (1.1) is not independent of additional terms that scale as t^1 and t^0. Dependence on such additional terms can be minimized by measuring α from the time-derivative $\dot{h} = 4\alpha Agt$ instead. Thus, as a confirmation, the "instantaneous" value of $\alpha = \dot{h}/(4Agt)$ is also shown in figure 6, where a self-similar, asymptotic value of α = 0.086 ± 0.01 is measured for $\tau \geq 1.1$. While this measure of α has a larger degree of statistical uncertainty due to the time-derivative of h, both values of α are consistent. The growth parameter for the salt/fresh water case is slightly larger than that for the hot/cold water case, where $\alpha = 0.07 \pm 0.011$ (Snider & Andrews 1994). Thus, the increase in the growth parameter α for the salt/fresh water case suggests that the Schmidt number may have only a minor influence on the late time growth rate of the mixing layer width.

3.2 *Measurements of chemical product formation*

Using the backlit optical techniques described in § 2.2, the average concentration of the colored chemical indicator was measured in a turbulent Rayleigh–Taylor mixing layer. Figure 4 shows an image of the layer, where the pink chemical indicator represents regions of mixed fluid. Figure 7 shows the profiles of $C = \overline{[\mathrm{In}_{\mathrm{IV}}]}/[\mathrm{In}]_2$ (the concentration of colored indicator normalized by the free stream concentration) for pH_2 = 7.02 and pH_2 = 2.44. The resulting profiles are approximately parabolic and, as expected, less chemical product is produced in the latter case. By decreasing the pH of the bottom stream, the concentration of H^+ ions is increased, so that the quantity of OH^- ions required to mix with the bottom stream to achieve a color change in the indicator is increased. Therefore, given the same degree of molecular mixing between the two streams, less colored indicator is produced when the pH of the bottom stream is lowered. In the pH_1 = 7.02 and pH_2 = 2.44 cases, the measured concentration of the colored indicator increases as the mixing layer grows spatially downstream. This is expected, as the intensity of turbulence increases and the internal structure of the mixing layer becomes more complex with increasing Reynolds numbers. Turbulent fluctuations continuously stretch the interface between pockets of fresh and salt water, which increases the reaction surface area and brings fresh reactants into contact.

Previous researchers have found that the quantity of indicator produced is a function of the equivalence ratio φ, and is a measure of balance or excess of reactants. Typically, the equivalence ratio for shear and jet flows is defined for the reaction involving the chemical indicator [see (2.4)] such that

$$\varphi_{\mathrm{In}} = \frac{[\mathrm{In}]/[\mathrm{OH}^-]}{\left([\mathrm{In}]/[\mathrm{OH}^-]\right)_{st}}, \tag{3.2}$$

where $\left([\mathrm{In}]/[\mathrm{OH}^-]\right)_{st} = 1/2$ is the stoichiometric ratio of reactants in (2.4). In the limit $\varphi_{\mathrm{In}} \to 0$, the quantity of colored chemical indicator C produced attains an asymptotic value and is a function only of the degree of molecular mixing between the two fluids (Shea 1977; Breidenthal 1979, 1981; Mungal & Dimotakis 1984; Zhang *et al.* 1995).

The equivalence ratio for the indicator reaction neglects the neutralization reaction in (2.2) that occurs as fluid from each stream mixes. Accordingly, φ_{In} does not account for the reduced quantity of indicator formed in the $pH_2 = 2.44$ experiment. To account for this effect, it is more appropriate to examine the equivalence ratio of the neutralization reaction in (2.2), where

$$\varphi_n = \frac{[\mathrm{H}^+]/[\mathrm{OH}^-]}{\left([\mathrm{H}^+]/[\mathrm{OH}^-]\right)_{st}} \tag{3.3}$$

and $([\mathrm{OH}^-]/[\mathrm{H}^+])_{st} = 1$ is the stoichiometric ratio of hydroxide and hydrogen ions. The neutralization equivalence ratio φ_n controls the volume fractions of fluid 1 and fluid 2 that must mix to achieve the pH increase required for the indicator to change color. For $\varphi_n \to 0$, a large excess of OH^- ions exists in the top stream and only a small fraction of fluid 1 must mix with fluid 2 to achieve a significant pH increase and resulting indicator color change. Conversely, for $\varphi_n \to \infty$, a large excess of H^+ ions exists and an infinite amount of fluid 1 is required to mix with fluid 2 to achieve the required pH increase. As a result, no indicator will be converted to its colored form. For the pH combination $pH_1 = 11.5$ and $pH_2 = 7$, $\varphi_n = 3.2\times10^{-5} \ll 1$ and only a small fraction of fluid 1 is required to mix with fluid 2 to achieve a color change. Accordingly, a measure of C for $\varphi_{\mathrm{In}} = 1.8\times10^{-3}$ and $\varphi_n = 3.2\times10^{-5}$ ($pH_1 = 11.5$, $pH_2 = 7$, $[\mathrm{In}]_2 = 6 \times 10^{-6}$) should be insensitive to the exact equivalence ratio and representative of the degree of molecular mixing.

3.3 *Species diffusivity considerations*

In previous works examining high Schmidt number liquid-phase mixing (Breidenthal 1979, 1981; Koochesfahani & Dimotakis 1986; Linden *et al.* 1994; Zhang *et al.* 1995), acid-base neutralization reactions coupled with pH-sensitive chemical indicators quantified the degree of molecular mixing. While it is customary to estimate $Sc \sim 10^3$ in liquid-phase mixing, each specific molecule or ion within the mixture diffuses at a different rate. Table 1 lists the diffusivities of the species and their respective Schmidt numbers for the current experiments. It is important to note that the neutralization reaction front will precede the indicator reaction front

because of the relatively high diffusivities of H^+ and OH^-. Accordingly, the total quantity of colored indicator is not limited by the diffusivities of the H^+ and OH^- ions. Larger ions, such as those of sodium and chloride, have lower mobilities, resulting in an effective Schmidt number $Sc_{NaCl} = \nu/D_{NaCl} = 620$ (Lide 2006). The diffusivity of phenolphthalein was measured by Desai and Vadgama (1991), and give an indicator Schmidt number of $Sc_{In} = \nu/D_{In} = 1200$. Because of the difference in Sc_{NaCl} and Sc_{In}, the nominal Schmidt number of the experiments reported here is considered as $Sc \sim 10^3$.

An experiment was performed using a temperature increase in the bottom fluid stream ($\Delta T \approx 5^\circ$ C) to create a density difference in order to demonstrate that the diffusivity of the chemical indicator determines the nominal Schmidt number of the experiment. For this reference experiment, the pH of each stream was set to $pH_1 \approx 11.5$ and $pH_2 \approx 7$ to match φ_{In} and φ_n of the baseline salt/fresh water experiments. No salt was added to the top stream, and thus the temperature of the water becomes a marker for the density field through an equation of state (Kukulka 1981). In this arrangement, the nominal Schmidt number of the scalar marking the density field is $Pr = 7 \equiv Sc$; however, the Schmidt number for the chemical indicator remains unchanged at $Sc_{In} = 1200$. Measurements of the colored indicator concentration for this hot/cold water case are shown in figure 8. These profiles indicate that similar amounts of colored chemical product are produced, despite the increased scalar diffusivity and presumably increased amount of mixed fluid within the layer. This experiment demonstrates that the diffusivity of the indicator limits its use to flows where the diffusivities of the scalar marking the density field are similar to the diffusivity of the indicator. In the present experiments, the diffusivity of Na^+ and Cl^- ions in water give an effective Schmidt number $Sc_{NaCl} = 620$ (Lide 2006), which is a factor of two smaller than $Sc_{In} = 1200$. It will be shown in § 4.2 that a factor of 10 difference in Schmidt numbers results in only a small change in the measurement of the molecular mixing parameter θ, and thus, a factor of two difference in the Schmidt numbers of salt and phenolphthalein is negligible.

3.4 *Product thickness integrals*

An integral measure quantifying the amount of chemical product formed (and representing the fraction of the mixing layer occupied by the colored indicator) is the equivalent product thickness

$$\frac{P}{h} = \frac{1}{h} \int_{-h/2}^{h/2} \frac{\overline{[\mathrm{In_{IV}}]}}{[\mathrm{In}]_2} \, \mathrm{d}z \,, \tag{3.4}$$

which is analogous to P/δ for shear flows (Konrad 1977; Briedenthal 1979, 1981). For all experiments that used salt to create a density difference, a correction to (3.4) was applied to account for the absorption of light by the salt water from the measurement of P:

$$\frac{P}{h} = \frac{1}{h} \left[\int_{-h/2}^{h/2} \frac{\overline{[\mathrm{In_{IV}}]}}{[\mathrm{In}]_2} \, \mathrm{d}z - \frac{h}{2} \xi \right], \tag{3.5}$$

where $\xi \approx 0.0075$ is the value of C measured outside the mixing layer in the salt water stream.

To validate the diagnostic techniques described in § 2.2, the water channel was used to create a reacting, turbulent shear layer similar to the flow created by Breidenthal (1979, 1981). The pH of each stream was set to $\mathrm{pH}_1 = 11.73$ and $\mathrm{pH}_2 = 7.04$ to match Breidenthal's conditions. The indicator concentration was set to $[\mathrm{In}]_2 = 5 \times 10^{-6}$ M, whereas Breidenthal used $[\mathrm{In}]_2 = 1 \times 10^{-5}$ M. The indicator concentration in the current experiments was lowered to keep the diagnostics in the linear range of the calibration. Salt was also added to the bottom stream as necessary to balance the increased density of the top stream due to the addition of NaOH, so that $\rho_1 = \rho_2$. The velocities of the top and bottom streams in the channel were adjusted to $U_1 = 5.8$ and $U_2 = 3.5$ cm/s, respectively, giving a velocity ratio $r = U_2/U_1 = 0.61$. While Breidenthal reported results for $r = 0.38$–0.80, the absolute velocities of each stream were much larger than those used in the current water channel. In Breidenthal's work, the high speed stream was $U_1 = 300$ cm/s, with a resulting low speed stream velocity $U_2 = rU_1$. In addition, Breidenthal's facility used a series of flow straighteners and meshes, and included a large cross-sectional area contraction to minimize boundary layers on the splitter plate and adjustable side walls to account for streamwise pressure gradients. The current water channel experiments also use a series of

flow-straighteners and screen meshes to control boundary layers on the splitter plate, but no contraction was implemented. Due to differences in facility designs and flow velocities, the initial conditions for each experiment are not expected to be identical. Breidenthal reported that P/δ is a non-unique function of Reynolds number for $Re_\delta < 8000$. This was attributed to the observation that early-time, two-dimensional vorticity dynamics of the mixing layer was controlled by the initial vorticity in the high-speed fluid boundary layer. Remnants of initial conditions affected the value of P/δ until the mixing layer had completely transitioned to a fully-developed, three-dimensional state. Thus, slightly different initial conditions resulted in different measures of P/δ before the asymptotic value $P/\delta \approx 0.365$ for $Re_\delta > 8000$ was reached.

Figure 9 shows a comparison of P/δ for $r = 0.62$ and $r = 0.76$ from Breidenthal (1979) and a corresponding shear layer experiment conducted in the current water channel as a function of shear layer Reynolds number $Re_\delta = \Delta U\,\delta/\nu$, where $\delta = \Delta U/(\partial u/\partial z)_{max}$ is the width (vorticity thickness) of the shear layer. In the absence of velocity measurements to obtain δ directly, the width of the shear layer was determined visually from the measured indicator concentration profiles. The visual width of the mixing layer, δ_{vis}, is related to the vorticity thickness δ such that $\delta_{vis}/\delta = 2.1$ (Brown & Roshko 1974; Koochesfahani & Dimotakis 1986). The water channel Reynolds numbers were limited to $Re_\delta < 2000$. Thus, the asymptotic value of $P/\delta \rightarrow 0.365$ for $Re_\delta > 8000$ observed by Breidenthal could not be reproduced in our channel; however, over the range of comparable Reynolds numbers shown in figure 9, our measurements of P/δ are within the scatter of Breidenthal's results for comparable velocity ratios.

A measurement of the relative product thickness for the Rayleigh–Taylor case, denoted P/h, is shown in figure 10. For Rayleigh–Taylor mixing layers, any Reynolds number definition relies upon a choice of an integral-scale velocity and length. This work adopts $Re_h = 0.35\sqrt{A\,g\,h^3}/\nu$ (Ramaprabhu & Andrews 2004), where the mixing layer width (5–95% volume fraction thresholds used) is the length-scale, and the terminal velocity of the dominant bubble is the velocity-scale. It is difficult to directly compare shear-driven mixing layers with the buoyancy-driven case due to the difference in Reynolds number definitions. For Rayleigh–Taylor

mixing layers, the visual width of the layer defined the integral length scale that in-turn was used to define h, and hence P/h and Re_h. Thus, for comparison purposes in figure 10, the shear layer Reynolds numbers and product thicknesses have been defined using δ_{vis} instead of δ. For the shear layer cases in figure 10, it is evident that the Reynolds number at which a significant rise in P/δ_{vis} occurs is a function of the Reynolds number, velocity ratio, and initial conditions. While the Reynolds number definitions are not completely equivalent for the buoyancy- and shear-driven cases, their comparison in figure 10 shows that the buoyancy-driven case exhibits an increasing trend in P/h, indicative of the onset of turbulence and a mixing transition at similar Reynolds numbers as the shear-driven case. However, higher Reynolds number experiments are needed to determine if buoyancy-driven turbulent mixing is capable of producing larger quantities of chemical product, and if P/h attains an asymptotic value. Extrapolation from the shear-driven experiments suggests that an asymptotic behavior of P/h may not be seen in Rayleigh–Taylor mixing until $Re_h \approx 8000$–10000, necessitating a different experimental facility for investigating asymptotic $Sc \sim 10^3$ mixing.

4. Measurements of molecular mixing

The backlit optical technique described in § 2.2 provided measurements of the average concentration of colored indicator $\overline{[\mathrm{In}_{\mathrm{IV}}]}$ given two streams at pH_1 and pH_2. While these measurements of chemical product formation are a function of the degree of molecular mixing at small equivalence ratios, it is desirable to relate C to more convenient measures of molecular mixing. In this section, the measured passive scalar and reacting scalar concentration field, $\overline{f}_1$ and C respectively, will be used to compute several parameters that quantify mixing.

4.1 *Measurements of product formation mixing parameter*

The measured indicator concentration profiles can be used to compute integral measures of the total quantity of chemical product formed, such as P/h. However, such a measure does not indicate the maximum quantity of chemical product that may be formed for the same equivalence ratio. Koochesfahani and Dimotakis (1986) quantified the degree of mixing in a reacting shear

layer by normalizing the amount of product formed by the maximum product that could be formed if the two fluids homogeneously mixed. Cook and Dimotakis (2001) extended this concept to define an integral mixing parameter

$$\Xi(\varphi_{\mathrm{In}}) = \frac{\int \overline{[\mathrm{In_{IV}}]}\,\mathrm{d}z}{\int \overline{[\mathrm{In_{IV}}]}_{max}\,\mathrm{d}z}, \tag{4.1}$$

where $\overline{[\mathrm{In_{IV}}]}_{max}$ is the maximum chemical product that can be produced if all fluid within the mixing layer was homogeneously mixed at a set equivalence ratio φ_{In}. This parameter is defined such that $\Xi = 0$ if no product is produced (*i.e.* the constituent fluids are completely segregated). Conversely, $\Xi = 1$ if all potential product has been produced (*i.e.* the mixing layer is homogeneously mixed). For the two-fluid case (where $\overline{f}_1 + \overline{f}_2 = 1$) $\overline{[\mathrm{In_{IV}}]}_{max}$ depends upon the lean reactant such that

$$\overline{[\mathrm{In_{IV}}]}_{max} = \begin{cases} \overline{f}_1[\mathrm{OH^-}]_1 & \overline{f}_1 \le (\overline{f}_1)_{st} \\ \left(1-\overline{f}_1\right)[\mathrm{In}]_2 & \overline{f}_1 > (\overline{f}_1)_{st} \end{cases}, \tag{4.2}$$

where

$$(\overline{f}_1)_{st} = \frac{\varphi_{\mathrm{In}}}{1+\varphi_{\mathrm{In}}} \tag{4.3}$$

is the stoichiometric volume fraction of fluid 1 required to achieve a stoichiometric reaction, *i.e.* all reactants in (2.4) are entirely consumed. An illustration of the maximum product produced for a given equivalence ratio is shown in figure 11. The global mixing parameter Ξ is shown in figure 18, where it is compared with the global mixing parameter Θ, defined in § 4.3.

4.2 *Relationship between chemical product formation measurements and fluctuating density statistics*

Measurements of the relative quantity of chemical product formed (given by Ξ) are dependent upon the equivalence ratio φ_{In}. An alternative description of molecular mixing is given by a combination of the mean and fluctuating density statistics, which are independent of the equivalence ratio. The mean density and density variance can be combined to form a molecular mixing parameter

$$\theta = 1 - \frac{B_0}{B_2} = 1 - \frac{\overline{f_1'^2}}{\bar{f}_1 \bar{f}_2}, \tag{4.4}$$

where $B_0 = \overline{\rho'^2} \big/ (\Delta\rho)^2 = \overline{f_1'^2}$ is a measure of the density variance, $\Delta\rho = \rho_1 - \rho_2$, and $B_2 = \bar{f}_1 \bar{f}_2$ is the limiting value of B_0 for the case of immiscible fluids, with $f_1 = 1 - f_2$ and $\overline{f_1'^2} = \overline{f_2'^2}$ by symmetry in a two-fluid mixture. Thus, $\theta = 0$ if the two fluids are completely unmixed (*i.e.* immiscible fluids), and $\theta = 1$ if the two fluids are completely molecularly mixed. This parameter has been reported by various researchers (Youngs 1984; Dalziel *et al.* 1999; Wilson & Andrews 2002; Ramaprabhu & Andrews 2004; Ristorcelli & Clark 2004; Mueschke *et al.* 2006) and provides a practical measure of molecular mixing as transport equations for $\bar{f}_1$ and $\overline{f_1'^2}$ can be derived, modeled, and solved to predict mixing (Chassaing *et al.* 2002; Veynante & Vervisch 2002; Fox 2003).

The formation of colored chemical product can be related to the volume fraction variance $\overline{f_2'^2}$, or more specifically, the second moment of the volume fraction probability density function (PDF), where $\overline{f_2^2} = \left(\bar{f}_2\right)^2 + \overline{f_2'^2}$. Given a mixture with varying density (such as within a Rayleigh–Taylor mixing layer), the probability of finding a given fraction of fluid *r* is quantified by the PDF of the volume fraction fluctuations $P(f_2)$. Using $P(f_2)$, the quantity of chemical indicator and fraction of colored indicator within the mixing layer can be expressed as functions of the local fluid composition, *i.e.* the PDF of f_2. As noted earlier, fluid 1 is the heavier fluid with a pH > 7 (alkali) and fluid 2 is the lighter fluid with pH ≤ 7 (acidic or neutral) with a dilute amount of phenolphthalein added. Accordingly, the average concentration of indicator present within the mixing layer depends upon the indicator concentration in the lighter fluid (bottom stream) $[\mathrm{In}]_2$ and $\bar{f}_2$, which is equivalent to the first moment of $P(f_2)$,

$$\overline{[\mathrm{In}]} = [\mathrm{In}]_2 \int_0^1 f_2 \, P(f_2) \, \mathrm{d}f_2 \, . \tag{4.5}$$

The total amount of indicator that is in its colored form depends on both the fraction of fluid 2 present and the fraction of dissociation $\alpha_{\mathrm{In_{IV}}}$ [see (2.12)]. Similar to (4.5), the concentration of colored indicator is expressed as

$$\overline{[\mathrm{In_{IV}}]} = [\mathrm{In}]_2 \int_0^1 \alpha_{\mathrm{In_{IV}}}(\mathrm{pH})\, f_2\, P(f_2)\, \mathrm{d}f_2 \,. \tag{4.6}$$

Consequently, $C = \overline{[\mathrm{In_{IV}}]} / [\mathrm{In}]_2$ can be expressed as a function of the local composition of the mixed fluid, or $P(f_2)$. To relate C and $\overline{f_2^2}$, the integral on the right-hand side of (4.6) requires further evaluation.

While the right-hand side of (4.6) cannot be analytically evaluated, an approximation for $\alpha_{\mathrm{In_{IV}}}$ can be obtained to allow an analytical treatment. If pH_1 is taken to be sufficiently large ($\mathrm{pH}_1 \approx 11.5$ here), then $\alpha_{\mathrm{In_{IV}}}$ becomes a function only of the local composition of the fluid, defined by f_1, f_2, and pH_2. Only two-fluid systems are considered here, so that $\alpha_{\mathrm{In_{IV}}}$ is a function of only f_2 and pH_2. As pH_2 is decreased, a larger quantity of OH^- ions from the top stream is required [see φ_n in (3.3)], and hence a greater value of f_1, to mix with the bottom stream to achieve the same rise in pH and indicator color change. Figure 12 shows $\alpha_{\mathrm{In_{IV}}}(f_2, \mathrm{pH}_2)$ as a function of local volume fraction f_2 with pH_2 as a parameter. The fraction of dissociation is then approximated by a step function

$$\alpha_{\mathrm{In_{IV}}}(f_2, f_2^{50\%}) = \begin{cases} \alpha_{\mathrm{In_{IV}}}^{max} = \alpha_{\mathrm{In_{IV}}}(\mathrm{pH} = 11.5) = 0.96 & f_2 \le f_2^{50\%}; \\ 0 & f_2 > f_2^{50\%}, \end{cases} \tag{4.7}$$

where $f_2^{50\%}$ is the f_2 value where half of the indicator exists in its colored form, *i.e.* $\alpha_{\mathrm{In_{IV}}} = 0.5$, for a specified $\mathrm{pH}_1/\mathrm{pH}_2$ combination. Note that $\alpha_{\mathrm{In_{IV}}}^{max} = 0.96$ because $\alpha_{\mathrm{In_{IV}}}$ does not attain unity at its maximum.

Substituting (4.7) into (4.6) allows the integral to be split into two parts and simplified:

$$\begin{aligned} C(f_2^{50\%}) &= \int_0^{f_2^{50\%}} \alpha_{\mathrm{In_{IV}}}(f_2, f_2^{50\%})\, f_2\, P(f_2)\, \mathrm{d}f_2 + \int_{f_2^{50\%}}^1 \alpha_{\mathrm{In_{IV}}}(f_2, f_2^{50\%})\, f_2\, P(f_2)\, \mathrm{d}f_2 \\ &= \alpha_{\mathrm{In_{IV}}}^{max} \int_0^{f_2^{50\%}} f_2\, P(f_2)\, \mathrm{d}f_2 \,. \end{aligned} \tag{4.8}$$

Integrating over all values of $f_2^{50\%}$ gives

$$\frac{1}{\alpha_{\mathrm{In_{IV}}}^{max}} \int_0^1 C(f_2^{50\%})\, \mathrm{d}f_2^{50\%} = \int_0^1 \left\{ \int_0^{f_2^{50\%}} f_2\, P(f_2)\, \mathrm{d}f_2 \right\} \mathrm{d}f_2^{50\%} \,. \tag{4.9}$$

Then, changing the order of integration on the right-hand side gives

$$\begin{aligned}\frac{1}{\alpha_{\mathrm{In_{IV}}}^{max}}\int_0^1 C(f_2^{50\%})\,\mathrm{d}f_2^{50\%} &= \int_0^1 \left\{ \int_{f_2}^1 f_2\,P(f_2)\,\mathrm{d}f_2^{50\%} \right\} \mathrm{d}f_2 \\ &= \int_0^1 f_2\,P(f_2) \left\{ f_2^{50\%}\Big|_{f_2}^1 \right\} \mathrm{d}f_2 \\ &= \int_0^1 (1-f_2)\,f_2\,P(f_2)\,\mathrm{d}f_2\end{aligned} \tag{4.10}$$

and evaluating the remaining outer integral gives

$$\frac{1}{\alpha_{\mathrm{In_{IV}}}^{max}}\int_0^1 C(f_2^{50\%})\,\mathrm{d}f_2^{50\%} = \overline{f}_2 - \overline{f_2^2}\,. \tag{4.11}$$

Since $\overline{f_2^2} = \left(\overline{f}_2\right)^2 + \overline{f_2'^2}$, the volume fraction variance becomes

$$\overline{f_2'^2} = \overline{f}_1\overline{f}_2 - \frac{1}{\alpha_{\mathrm{In_{IV}}}^{max}}\int_0^1 C(f_2^{50\%})\,\mathrm{d}f_2^{50\%}\,, \tag{4.12}$$

and the degree of molecular mixing becomes

$$\theta = 1 - \frac{\overline{f_1'^2}}{\overline{f}_1\,\overline{f}_2} = \frac{\int_0^1 C(f_2^{50\%})\,\mathrm{d}f_2^{50\%}}{\alpha_{max}\,\overline{f}_1\,\overline{f}_2}\,. \tag{4.13}$$

At the centerplane of the mixing layer, $\overline{f}_1 = \overline{f}_2 = 1/2$, and θ reduces to

$$\theta = \frac{4}{\alpha_{\mathrm{In_{IV}}}^{max}}\int_0^1 C(f_2^{50\%})\,\mathrm{d}f_2^{50\%}\,. \tag{4.14}$$

The integral of $C(f_2^{50\%})$ over $0 \le f_2^{50\%} \le 1$ in (4.12) may be physically interpreted as a sum of the chemical product produced given all possible equivalence ratios. Before this integral is quantified for the flow considered here, several considerations regarding the bounding values of $C(f_2^{50\%})$ at $f_2^{50\%} = 0$ and $f_2^{50\%} = 1$ are discussed. For highly acidic streams, $[\mathrm{H^+}]_2 \to \infty$ or $f_2^{50\%} \to 0$, and thus, no chemical indicator will exist in its colored form, *i.e.* $C(f_2^{50\%} = 0) = 0$. For the case of $\mathrm{pH_1} = \mathrm{pH_2} = 11.5$, $f_2^{50\%} = 1$ and no fluid from the top stream is required to mix with the bottom stream to achieve a color change. Then, the chemical indicator acts as a passive scalar, such that

$$\begin{aligned}\overline{[\mathrm{In_{IV}}]} &= [\mathrm{In}]_2 \int_0^1 \alpha_{\mathrm{In_{IV}}}(\mathrm{pH})\, f_2\, P(f_2)\, \mathrm{d}f_2 \\ &= \alpha_{\mathrm{In_{IV}}}^{max}\, [\mathrm{In}]_2\, \overline{f}_2 .\end{aligned} \tag{4.15}$$

Thus, the two bounding values $C(f_2^{50\%}=0)$ and $C(f_2^{50\%}=1)=\alpha_{\mathrm{In_{IV}}}^{max}\,\overline{f}_2$ are known *a priori*. To approximate the integral of $C(f_2^{50\%})$, the amount of colored product has been measured for $\mathrm{pH_2} = 7.02$ and $\mathrm{pH_2} = 2.44$. Keeping $\mathrm{pH_1} \approx 11.5$, this results in $f_2^{50\%}=0.986$ and $f_2^{50\%}=0.471$, respectively. Several curves of $C(f_2^{50\%})$ are shown for various evolution times in figure 13, using the chemical product measurements shown in figure 7.

4.3 *Measurement of molecular mixing parameters*

The terms on the right-hand side of (4.12), which include mean volume fraction and mean chemical indicator product profiles, have been measured and are shown in figures 5, 7, and 13. Combining these measured concentration profiles according to (4.12) provides a measure of the volume fraction variance profiles shown in figure 14 across the mixing layer from $\overline{f}_1 = 0.1$ to $\overline{f}_1 = 0.9$. The 10–90% volume fraction boundaries were used because measurements near the edges of the mixing layer are not converged due to a high degree of intermittency. The profiles in figure 14 are approximately parabolic in shape with peaks at the centerplane of the mixing layer. The magnitude of $\overline{f_1''^2}$ on the centerplane (z = 0) has bounding values of 0 (perfectly mixed) and 0.25 (perfectly segregated). As the mixing layer grows, $\overline{f_1''^2}(z=0)$ decreases in time, moving away from the immiscible limiting value of 0.25, which indicates a greater quantity of mixed fluid exists at later times.

The profiles of $\overline{f_1''^2}$ alone do not quantify the relative degree of molecular mixing, but such a measure is given by θ [see (4.4)]. To obtain profiles of θ, the volume fraction fluctuations (shown in figure 14) are combined with the mean volume fraction profiles (shown in figure 5) according to (4.12). Profiles of θ across the mixing layer are shown in figure 15 plotted between the 10–90% volume fraction thresholds. For the small Atwood case considered here, the profiles of θ are expected to be approximately constant across the mixing layer, as found in the experiments of Wilson and Andrews (2002) and in numerical simulations (Youngs 1994;

Ristorcelli & Clark 2004). Indeed our measured profiles of θ in figure 15 are reasonably flat at later times across most of the mixing layer, and no conclusions can be drawn from the oscillations near the boundaries of the mixing layer because of increased uncertainty due to intermittency effects away from the centerplane.

Uncertainties in $\overline{f_1'^2}$ and θ are given by a combination of the uncertainties in the mean volume fraction measurement and indicator concentration measurements. Uncertainties in the mean Nigrosine dye concentration measurements [as a result of (2.18)] contribute to uncertainties in the measured profiles of $\overline{f}_1$ and $\overline{f}_2$. Similarly, uncertainties in the mean chemical indicator concentration profiles contribute to uncertainties in the integral of (4.11). Combined, the relative uncertainty in $\overline{f_1'^2}$ is less than ±5% within the core of the mixing layer. However, the statistical uncertainty in the $\overline{f_1'^2}$ measurements increases near the mixing layer boundaries due to a greater degree of intermittency. Combining the uncertainties in the mean and fluctuating volume fraction statistics gives a relative measure of the uncertainty in the measurement of θ. Along the mixing layer centerplane, the absolute uncertainty in θ remains relatively unchanged for all times measured ($0.1 < \tau < 1.9$) at approximately $w_\theta \approx \pm 0.015$. While this is a modest absolute uncertainty, the relative uncertainty is large at early times due to the small values of θ. Away from the centerplane, the uncertainty estimates in θ increase to $w_\theta \approx \pm 0.05$. Profiles of the relative uncertainties for $\overline{f_1'^2}$ and θ are shown in figure 16.

Measurements of θ along the centerplane ($z = 0$) of the mixing layer have been reported in previous water channel experiments (Wilson & Andrews 2002; Ramaprabhu & Andrews 2004; Mueschke *et al.* 2006) and in gas channel experiments (Banerjee *et al.* 2007). The current centerplane measurements of θ are plotted in figure 17 with measurements from the gas channel where $Sc = 0.7$ (Banerjee *et al.* 2007), and the water channel for the hot/cold water case where $Pr \equiv Sc = 7$ (Mueschke *et al.* 2006). Inspection of figure 17 reveals that a factor of 10 difference in Schmidt/Prandtl numbers (0.7 to 7) between the water and gas channel experiments gives a small difference in θ over $0.5 < \tau < 1.5$. However, comparison of the moderate Schmidt number $Sc \sim 1$ results with the new $Sc \sim 10^3$ measurements results in a much larger and distinct

difference. In particular, the minimum value of $\theta \approx 0.4$ was measured in the hot/cold water experiments at $\tau = 0.4$ before the mixing layer had transitioned to a fully three-dimensional, turbulent mixing layer. A similar value of $\theta \approx 0.4$ was only measured in the salt/fresh water experiments when the mixing layer reached $Re_h \approx 2000$ at $\tau = 1.5$. At the latest time measured ($\tau = 1.9$) $\theta \approx 0.5$, which begins to approach the late time values of θ measured in the water channel. Thus, our Rayleigh–Taylor measurements are similar to the shear layer results (Konrad 1977; Breidenthal 1979, 1981) indicating that the Schmidt number has a smaller effect on the degree of molecular mixing at higher Reynolds number.

Youngs (1994) introduced a global measure of mixing

$$\Theta = \frac{\int \overline{f_1 f_2}\,\mathrm{d}z}{\int \overline{f}_1 \overline{f}_2\,\mathrm{d}z} = 1 - \frac{\int \overline{f_1''^2}\,\mathrm{d}z}{\int \overline{f}_1 \overline{f}_2\,\mathrm{d}z}, \tag{4.16}$$

which is analogous to the mixing parameter Ξ defined in § 4.1. As for θ and Ξ, $\Theta = 0$ when the two fluids are completely segregated, and $\Theta = 1$ when the two fluids are perfectly mixed. The mixing progress variables $\Xi(\varphi_{\mathrm{In}} \to 0)$ and Θ have been obtained from the present salt/fresh water experiments by integrating across the 10–90% volume fraction thresholds. The evolution of Ξ and Θ is shown in figure 18. At times $\tau < 0.4$, $\Xi < 0.06$ and $\Theta < 0.15$, indicating that the majority of the fluid within the mixing layer exists as pockets of pure fluid that are stirred, but not molecularly mixed. Just as with the evolution of θ shown in figure 17, both parameters increase and reach late time values $\Xi \approx 0.28$ and $\Theta \approx 0.5$, but neither appear to attain asymptotic values by $\tau = 1.9$. In comparison, Ramaprabhu, Dimonte and Andrews (2005) reported late-time values of $\Theta \approx 0.7$–0.8, where monotone-integrated large-eddy simulations (MILES) were used to examine the influence of initial conditions on molecular mixing. Using a large-eddy simulation, Cook, Cabot and Miller (2004) obtained $\Theta \approx 0.78$ for a moderate Atwood number ($A = 0.5$), $Sc = 1$ mixing layer. Thus, it is unclear whether θ or Θ in the $Sc \sim 10^3$ case reach the same asymptotic values measured in $Sc \sim 1$ experiments.

As shown in figure 10, the relative fraction of chemical product formed remains small

until the onset of a fully-turbulent regime, or equivalently, the Reynolds number attains sufficient magnitude. This effect can be seen clearly in figure 18, where a transition in the slopes of Θ and Ξ occurs at $\tau \approx 0.5$. Before this transition point, both Θ and Ξ exhibit shallow, approximately linear slopes. Following this transition ($\tau > 0.5$) the slopes of Θ and Ξ increase, indicating that the production rate of mixed fluid has increased. The weak effect of the Reynolds number before $\tau \approx 0.5$ is because the mixing layer contains little three-dimensional structure and is in a weakly nonlinear regime. However, as the bandwidths of velocity and spatial scales increase, stretching of the interface between the two fluids increases both the surface area and concentration gradients driving molecular diffusion. This Reynolds number effect on θ, Θ, and Ξ is shown more clearly in figure 19. As functions of Re_h, it is evident in figure 19 that the centerplane evolution of θ also exhibits the transition in slope at $\tau \approx 0.5$, corresponding to an integral-scale Reynolds number $Re_h \approx 300$.

As seen in the shear layer results of Konrad (1977) and Breidenthal (1979; 1981), a second transition is expected in the large Reynolds number limit, when each mixing parameter is expected to asymptote. Ristorcelli and Clark (2004) reported that the centerplane value of $\overline{f_1'^2}$ (and as a result θ) must be constant under the assumption of self-similarity. Approximately asymptotic behavior in θ at the centerplane was observed in the $Sc = 0.7$ gas-phase experiments (Banerjee *et al.* 2007) and in $Pr = 7$ liquid-phase experiments (Mueschke *et al.* 2007). Dalziel *et al.* (1999) used light-induced fluorescence (LIF) in a set of retracting plate experiments in a $Sc \sim 10^3$ salt/fresh water experiment and measured an approximately constant value $\Theta \approx 0.55$ over the range $0.4 < \tau < 1.5$ (when scaled to match the time normalization used in this work). However, LIF measurements are not resolution independent. The Batchelor scale for the analogous salt/fresh water experiments reaches $\eta_B = h\,Sc^{-1/2}Re^{-3/4} \approx 20$ μm, and thus, under-resolved pointwise concentration measurements will over-predict the degree of molecular mixing (Mueschke & Andrews 2005). In the present work, where the measurement technique is free of optical resolution constraints, no such asymptotic behavior of the mixing parameters is observed by the largest Reynolds numbers achieved, $Re_h \approx 3000$. From figure 10, if buoyancy-driven

mixing layers have an asymptotic value of P/h similar to that in shears layers, then an asymptotic behavior of θ and Θ in the $Sc \sim 10^3$ mixing layers may not be observed until $Re_h \approx 8000$–10000.

5. Implications for turbulent transport and mixing modeling

Mathematical models of turbulent transport and mixing are designed to predict large-scale observables, such as the mixing layer width h and its late-time growth rate α. In addition, to predict the relative degree of mixing, such models must also accurately predict second-order turbulence statistics, including the turbulent kinetic energy and density variance. These quantities have been an important subject of study in the reacting and combustion flow communities (Fox 2003; Poinsot & Veynante 2005), but have thus far received little attention in the Rayleigh–Taylor community. Anisotropy effects, statistical inhomogeneity, and nonequilibrium physics in Rayleigh–Taylor mixing layers also complicate the modeling process. Predictive models should also encompass a large dynamic Reynolds number range. As shown in figure 19, mixing models must capture the small mixing rate (shallow slope of θ and Θ) at $Re_h < 300$. At higher Reynolds numbers, these models must account for an increased mixing rate, the expected self-similar collapse of the volume fraction variance profiles shown in figure 20, and the eventual asymptotic behavior of P/h, θ, and Θ. This suggests that the model parameters in the production and dissipation terms in the modeled density variance $\overline{\rho'^2}$ (or equivalently $\overline{f_1'^2}$) transport equation may strongly depend on an integral-scale Reynolds number Re_h or a turbulent Reynolds number $Re_t = K^2/(\nu\varepsilon)$, where K and ε are the turbulent kinetic energy and its dissipation rate, respectively. Liu and Fox (2006) addressed this issue by analytically integrating model scalar spectra to determine the relationship between mechanical and scalar time-scales as a function of Re_t and Sc. However, the model proposed by Liu and Fox (2006) implies that the integral length scale is set by the bounding geometry (rather than the flow), which is not the case in Rayleigh–Taylor driven mixing. In addition, the model kinetic energy and scalar variance spectra neglect spectral nonequilibrium effects (Pope 2000; Fox 2003). Thus, the dependence of the mixing rate on the initial perturbations at the fluid interface cannot be incorporated, which has been shown to

have persisting effects out to at least $Re_h > 10^3$ (Cook & Dimotakis 2001; Ramaprabhu *et al.* 2005; Mueschke *et al.* 2006).

Accordingly, a complete calibration of transport models for high Schmidt Rayleigh–Taylor mixing requires measurements of transport quantities such as $\overline{f_1}$ and $\overline{f_1'^2}$. However, there is currently little detailed data available from direct numerical simulations (DNS) and experiments (compared with shear-driven turbulence) to aid in the calibration and validation of such models for Rayleigh–Taylor driven mixing. While DNS studies of Rayleigh–Taylor driven mixing are available at $Sc = 1$ (Cook & Dimotakis 2001; Ristorcelli & Clark 2004; Cabot & Cook 2006), no such data is available for the large Schmidt number case, for which DNS is too computationally expensive. In addition, there are few subgrid-scale models suitable for large-eddy simulation (LES) of large Schmidt number mixing (Pullin 2000). Furthermore, monotone-integrated large-eddy simulation (MILES) and implicit large-eddy simulation (ILES) do not include molecular dissipation and diffusion terms [having a numerical Schmidt number of $\mathcal{O}(1)$] and are thus poorly-suited to investigating Schmidt number effects on molecular mixing. Thus, the results of this work presently provide the sole experimental data for calibrating density variance transport models for high Schmidt number Rayleigh–Taylor mixing.

6. Conclusions

Experiments measuring the degree of molecular mixing in a liquid-phase, high Schmidt number Rayleigh–Taylor instability-driven mixing layer have been performed using a salt/fresh water configuration in a water channel. The measured mixing layer growth parameter $\alpha = 0.085 \pm 0.005$ for this salt/fresh water case indicates that the Schmidt number may have a minor influence on the late-time self-similar growth rate of the mixing layer width. To quantify the degree of molecular mixing, the pH of each water stream was altered, and a diffusion-limited neutralization reaction was monitored by the addition of a pH-sensitive chemical indicator. For the limiting case of the equivalence ratio $\varphi_{\mathrm{ln}} \to 0$, the chemical indicator concentration profiles indicate the degree of molecular mixing between the two fluids. As the buoyancy-driven mixing

developed, the quantity of chemical indicator measured continued to increase, showing that the quantity of mixed fluid within the turbulent core of the mixing layer continued to increase with time. Novel measurements of equivalent product thickness were reported, where at late times, P/h continues to increase with Reynolds number. The onset of a turbulent transition at $Re_h \approx Re_{\delta_{vis}} > 10^3$ was demonstrated by the increased rate of chemical product formation. However, the final mixing transition stage indicated by an asymptotic value of P/h, as seen in high Reynolds number shear flows, was not observed for $Re_h \leq 3000$.

New measurements of the degree of molecular mixing were reported using both the relative fraction of chemical product formed and fluctuating density statistics. Mathematical relationships between the measured mean passive scalar profiles, chemical indicator concentration profiles, and the density variance were developed. The first measurements of volume fraction variance profiles $\overline{f_1'^2}$ for $Sc \sim 10^3$ Rayleigh–Taylor mixing were obtained by integrating the total indicator formation over the range of equivalence ratios $0 < \varphi_n < \infty$ (or $0 < f_2^{50\%} < 1$). These profiles are approximately parabolic and the peak magnitude decreases in time, indicative of a greater volume of mixed fluid at later times. Combining measurements of $\overline{f}_1$ and $\overline{f_1'^2}$, a resolution-independent measurement of the molecular mixing parameter θ was obtained for the $Sc \sim 10^3$ case and compared with lower Schmidt number (0.7–7) experimental measurements. It was found that the increase in Schmidt number for the salt/fresh water experiments resulted in a significant decrease in θ for all times measured. In addition to the local mixing parameter θ, measurements of the global mixing parameters Ξ and Θ were also reported. Similar to θ, both Ξ and Θ were significantly lower than any values reported for $Sc \sim 1$ experiments and simulations. All parameters indicate an initial transition to a turbulent regime at $\tau \approx 0.5$ or $Re_h \approx 300$, where the initially-shallow linear slope of each parameter begins to increase. At the latest time, all of the molecular mixing parameters increased. It remains unclear whether the $Sc \sim 10^3$ mixing layers attain the same asymptotic value of θ as in lower Schmidt number Rayleigh–Taylor mixing experiments.

ACKLOWEDGEMENTS

This research was sponsored by the U.S. Department of Energy National Nuclear Security Administration under the Stewardship Science Academic Alliances program through DOE Research Grant #DE-FG03-02NA00060. This work was also performed under the auspices of U. S. DOE by Lawrence Livermore National Laboratory under Contract No. DE-AC52-07NA27344.

APPENDIX A. Neutralization chemistry

In aqueous solutions, the concentration of hydrogen and hydroxide ions satisfy the reversible reaction

$$\mathrm{H_2O} \rightleftharpoons \mathrm{H^+ + OH^-} \tag{7.1}$$

with an equilibrium constant

$$K_w = [\mathrm{H^+}][\mathrm{OH^-}] = 1\times 10^{-14}. \tag{7.2}$$

A mixture of two fluids with volume fractions f_1, f_2 and hydrogen ions concentrations pH_1, pH_2, will reach a new equilibrium value pH_{mix} as determined by conservation of mass and equilibrium constraints. The initial, unmixed ion concentrations are given by

$$a_0 = f_1[\mathrm{H^+}]_1 + f_2[\mathrm{H^+}]_2, \tag{7.3}$$

$$b_0 = f_1[\mathrm{OH^-}]_1 + f_2[\mathrm{OH^-}]_2, \tag{7.4}$$

which may not necessarily satisfy the equilibrium constraint in (7.2). Upon mixing, a_0 and b_0 will decrease by an amount x, giving final concentrations $a_{mix} = a_0 - x$ and $b_{mix} = b_0 - x$. The new equilibrium concentrations a_{mix} and b_{mix} must then satisfy the equilibrium constraint (7.2), where

$$\begin{aligned} K_w &= [\mathrm{H^+}][\mathrm{OH^-}] \\ &= (a_0 - x)(b_0 - x) \\ &= a_0 b_0 - x(a_0 + b_0) + x^2. \end{aligned} \tag{7.5}$$

The change in ion concentrations, x, can be calculated by solving the quadratic equation in (7.5), giving

$$x = \frac{(a_0 + b_0) - \sqrt{(a_0 + b_0)^2 - 4(a_0 b_0 - K_w)}}{2}, \tag{7.6}$$

where the negative root provides the physical solution. Accordingly, the final pH of the mixture is given by $\mathrm{pH}_{mix} = -\log_{10}(a_0 - x)$.

REFERENCES

ANUCHINA, N. N., KUCHERENKO, Y. A., NEUVAZHAEV, V. E., OGIBINA, V. N., SHIBARSHOV, L. I. & YAKOVLEV, V. G. 1978 Turbulent mixing at an accelerating interface between liquids of different densities. *Izv. Akad Nauk. SSSR, Mekh. Zhidk. Gaza* **6**, 157–160.

ATZENI, S. & MEYER-TER-VEHN, J. 2004 *The Physics of Inertial Fusion: Beam Plasma Interaction, Hydrodynamics, Hot Dense Matter*, International Series of Monographs on Physics Vol. 125. Oxford University Press.

BANERJEE, A. KRAFT, W. & ANDREWS, M. J. 2007 Detailed measurements of a Rayleigh–Taylor mixing layer from small to intermediate Atwood numbers. (*submitted*).

BENEDICT, L. H. & GOULD, R. D. 1996 Towards better uncertainty estimates for turbulence statistics. *Exp. Fluids* **22**, 129–136.

BETTI, R., UMANSKY, M., LOBATCHEV, V., GONCHAROV, V. N. & MCCRORY, R. L. 2001 Hot-spot dynamics and deceleration-phase Rayleigh–Taylor instability of imploding inertial confinement fusion capsules. *Phys. Plasmas* **8**, 5257–5267.

BISHOP, E. (editor) 1972 *Indicators.* International Series of Monographs in Analytical Chemistry: Indicators. Pergamon Press.

BREIDENTHAL, R. 1979. *A chemically reacting turbulent shear layer*. Ph.D. dissertation, California Institute of Technology.

BREIDENTHAL, R. 1981 Structure in turbulent mixing layers and wakes using a chemical reaction. *J. Fluid Mech.* **109**, 1–24.

BROWAND, F. K. & WEIDMAN, P. D. 1976 Large scales in the developing mixing layer. *J. Fluid Mech.* **76**, 127–144.

BROWN, G. L. & ROSHKO, A. 1974 On density effects and large structure in turbulent mixing layers. *J. Fluid Mech.* **64**, 775–816.

CHANDRASEKHAR, S. 1961 *Hydrodynamic and Hydromagnetic Stability*. Dover.

CHASSAING, P., ANTONIA, R. A., ANSELMET, F., JOLY, L. & SARKAR, S. 2002 *Variable Density Fluid Turbulence*. Fluid Mechanics and its Applications Vol. 69, Kluwer Academic.

COOK, A. W. & DIMOTAKIS, P. E. 2001 Transition stages of Rayleigh–Taylor instability between miscible fluids. *J. Fluid Mech.* **443**, 69–99. Corrigendum. *J. Fluid Mech.* **457**, 410–411 (2002).

COOK, A. W., CABOT, W. & MILLER, P. L. 2004 The mixing transition in Rayleigh–Taylor instability. *J. Fluid Mech.* **511**, 333–362.

CABOT, W. H. & COOK, A. W. 2006 Reynolds number effects on Rayleigh–Taylor instability with possible implications for type-Ia supernovae. *Nat. Phys.* **2**, 562–568.

CUI, A. Q. & STREET, R. L. 2004 Large-eddy simulation of coastal upwelling flow. *Envir. Fluid Mech.* **4**, 197–223.

DALZIEL, S. B., LINDEN, P. F. & YOUNGS, D. L. 1999 Self-similarity and internal structure of turbulence induced by Rayleigh–Taylor instability. *J. Fluid Mech.* **399**, 1–48.

DANKWERTS, P. V. 1952 The definition and measurement of some characteristics of mixtures. *Appl. Sci. Res.* **3**, 279–296.

DESAI, M. A. & VADGAMA, P. 1991 Estimation of effective diffusion coefficients of model solutes through gastric mucus: assessment of a diffusion chamber technique based on spectrophotometric analysis. *Analyst* **116**, 1113–1116.

DIMOTAKIS, P. E. 2005 Turbulent mixing. *Annu. Rev. Fluid Mech.* **37**, 329–356.

FOX, R. O. 2003 *Computational Models for Turbulent Reacting Flows*. Cambridge University Press.

GREEN, F. J. 1990 *The Sigma-Aldrich Handbook of Stains, Dyes, and Indicators*. Aldrich Chemical Co.

HAAN, S. W. 1989 Onset of nonlinear saturation for Rayleigh–Taylor growth in the presence of a full spectrum of modes. *Phys. Rev. A* **39**, 5812–5825.

HARRIS, D. C. 2003 *Quantitative Chemical Analysis*, sixth ed. W. H. Freeman and Company.

HECHT, E. 2002 *Optics*, fourth ed. Addison Wesley.

KOOP, G. K. 1976 *Instability and turbulence in a stratified shear layer.* Ph.D. dissertation. University of Southern California.

KOLTHOFF, I. M. 1937 *Acid-Base Indicators*. Macmillan.

KONRAD, J. H. 1977 *An experimental investigation of mixing in two-dimensional turbulent shear flows with applications to diffusion-limited chemical reactions.* Ph.D. dissertation, California Institute of Technology.

KOOCHESFAHANI, M. M. & DIMOTAKIS, P. E. 1986 Mixing and chemical reactions in a turbulent liquid mixing layer. *J. Fluid Mech.* **170**, 83–112.

KUKULKA, D. J. 1981 *Thermodynamic and transport properties of pure and saline water*. M.S. thesis, State University of New York at Buffalo.

LIDE, D. R. (editor) 2006 *CRC Handbook of Chemistry and Physics*, eighty-seventh ed. CRC Press.

LINDEN P. F. & REDONDO, J. M. 1991 Molecular mixing in Rayleigh–Taylor instability. Part I: Global mixing. *Phys. Fluids A* **3**, 1269–1277.

LINDEN P. F., REDONDO, J. M. & YOUNGS D. L. 1994 Molecular mixing in Rayleigh–Taylor instability. *J. Fluid Mech.* **265**, 97–124.

LINDL, J. D. 1998 *Inertial Confinement Fusion: The Quest for Ignition and Energy Gain using Indirect Drive*. Springer-Verlag.

LIU, Y. & FOX R. O. 2006 CFD predictions for chemical processing in a confined impinging-jets reactor. *AIChE J.* **52**, 731–744.

MARMOTTANT, P. H. & VILLERMAUX, E. 2004 On spray formation. *J. Fluid Mech.* **498**, 73–111.

MOLCHANOV, O. A. 2004 On the origin of low- and middler-latitude ionospheric turbulence. *Phys. Chem. Earth* **29**, 559–567.

MUESCHKE, N. J. & ANDREWS, M. J. 2005 Investigation of scalar measurement error in diffusion and mixing processes. *Exp. Fluids* **40**, 165–175; Erratum. *Exp. Fluids* **40**, 176 (2005).

MUESCHKE, N. J., ANDREWS, M. J. & SCHILLING, O. 2006 Experimental characterization of initial conditions and spatio-temporal evolution of a small-Atwood-number Rayleigh–Taylor mixing layer. *J. Fluid Mech.* **567**, 27–63.

MUNGAL, M. G. & DIMOTAKIS, P. E. 1984 Mixing and combustion with low heat release in a turbulent shear layer. *J. Fluid Mech.* **148**, 349–382.

POINSOT, T. & VEYNANTE, D. 2005 *Theoretical and Numerical Combustion*, second ed. R. T. Edwards.

POPE, S. B. 2000 *Turbulent Flows*. Cambridge University Press.

PULLIN, D. I. 2000 A vortex-based model for the subgrid flux of a passive scalar. *Phys. Fluids* **12**, 2311–2319.

RAMAPRABHU, P. & ANDREWS, M. J. 2004 Experimental investigation of Rayleigh–Taylor mixing at small Atwood numbers. *J. Fluid Mech.* **502**, 233–271.

RAMAPRABHU, P., DIMONTE, G. & ANDREWS, M. J. 2005 A numerical study of the influence of initial perturbations on the turbulent Rayleigh–Taylor instability. *J. Fluid Mech.* **536**, 285–319.

RAYLEIGH, LORD. 1884 Investigation of the equilibrium of an incompressible heavy fluid of variable density. *Proc. London Math. Soc.* **14**, 170–177.

RISTORCELLI, J. R. & CLARK, T. T. 2004 Rayleigh–Taylor turbulence: self-similar analysis and direct numerical simulations. *J. Fluid Mech.* **507**, 213–253.

SHEA, J. R. 1977 A chemical reaction in a turbulent jet. *J. Fluid Mech.* **81**, 317–333.

SMARR, L., WILSON, J. R., BARTON, R. T. & BOWERS, R. L. 1981 Rayleigh–Taylor overturn in super-nova core collapse. *Astrophys. J.* **246**, 515–525.

SNIDER, D. M. & ANDREWS, M. J. 1994 Rayleigh–Taylor and shear driven mixing with an unstable thermal stratification. *Phys. Fluids A* **6**, 3324–3334.

STILLINGER, D. C., HEAD, M. J., HELLAND, K. N. & VAN ATTA, C. W. 1983 A closed loop gravity-driven water channel for density stratified shear flow. *J. Fluid Mech.* **131**, 73–89.

TAYLOR, G. I. 1950 The instability of liquid surfaces when accelerated in a direction perpendicular to their planes. *Proc. Royal Soc. London* **201**, 192–196.

THOMAS, G. O. 2003 The aerodynamic breakup of ligaments. *Atom. Sprays* **13**, 117–129.

VEYNANTE, D & VERVISCH, L. 2002 Turbulent combustion modeling. *Prog. Energy Combust. Sci.* **28**, 193–266.

WARHAFT, Z. 2000 Passive scalars in turbulent flows. *Annu. Rev. Fluid Mech.* **32**, 203–240.

WILSON, P. N. & ANDREWS, M. J. 2002 Spectral measurements of Rayleigh–Taylor mixing at low-Atwood number. *Phys. Fluids A* **14**, 938–945.

YOUNGS, D. L. 1984 Numerical simulations of turbulent mixing by Rayleigh–Taylor instability. *Physica D* **12**, 32–44.

YOUNGS, D. L. 1994 Numerical simulation of mixing by Rayleigh–Taylor and Richtmyer–Meshkov instabilities. *Laser Part. Beams* **12**, 725–750.

ZHANG, S. & SCHNEIDER, S. P. 1995 Quantitative molecular-mixing measurements in a round jet with tabs. *Phys. Fluids* **7**, 1063–1070.

ZHANG, S., SCHNEIDER, S. P., COLLICOTT, S. H. 1995 Quantitative molecular-mixing measurements using digital processing of absorption images. *Exp. Fluids* **19**, 319–327.

TABLES

	Diffusivity [cm^2/s]	*Sc*
Na^+	1.334×10^{-5}	750
Cl^-	2.032×10^{-5}	492
NaCl	1.611×10^{-5}	620
H^+	9.311×10^{-5}	107
OH^-	5.273×10^{-5}	190
Phenolphthalein	8.3×10^{-6}	1200

TABLE 1. Species diffusivities in water at 20° C (Desai & Vadgama 1991; Lide 2006).

FIGURES

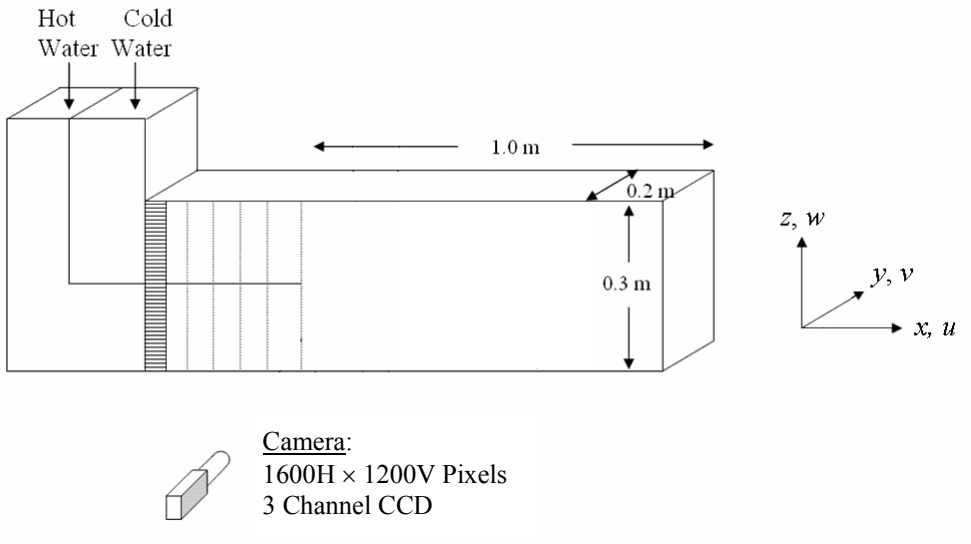

FIGURE 1. Schematic of the water channel and the associated coordinate system.

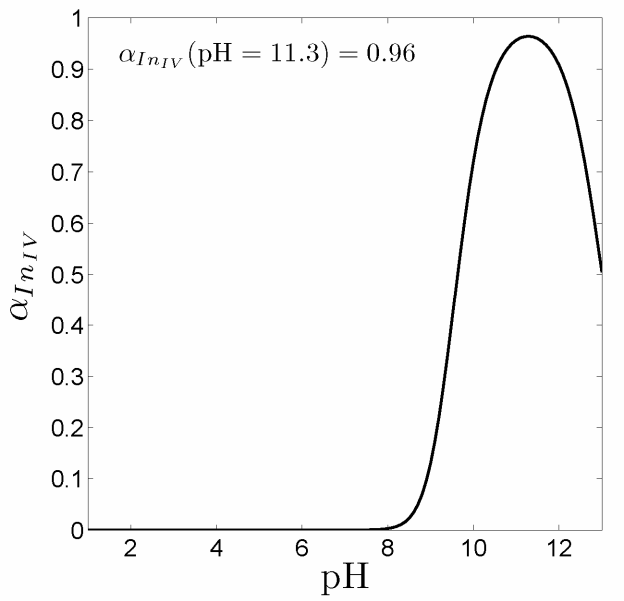

FIGURE 2. Fraction of dissociation for the colored form of the chemical indicator In_{IV}.

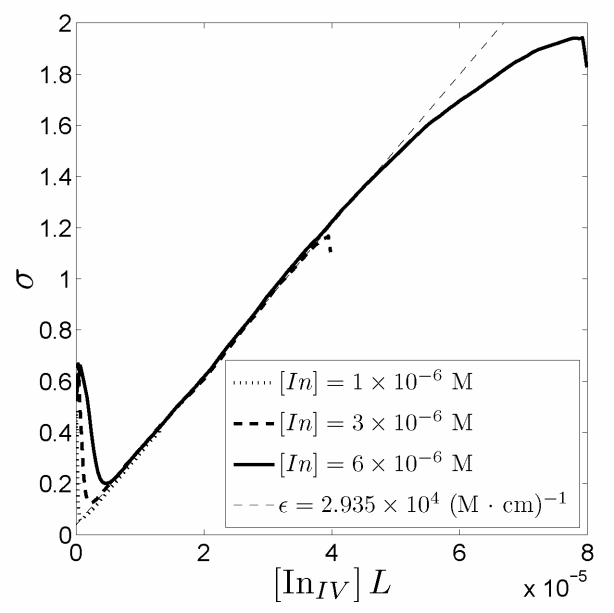

FIGURE 3. Calibration of molar absorptivity coefficient $\varepsilon_{\mathrm{In}}$ for phenolphthalein. A fiducial for $\varepsilon_{\mathrm{In}} = 2.935 \times 10^{-4}$ (M cm)$^{-1}$ is shown (dashed line).

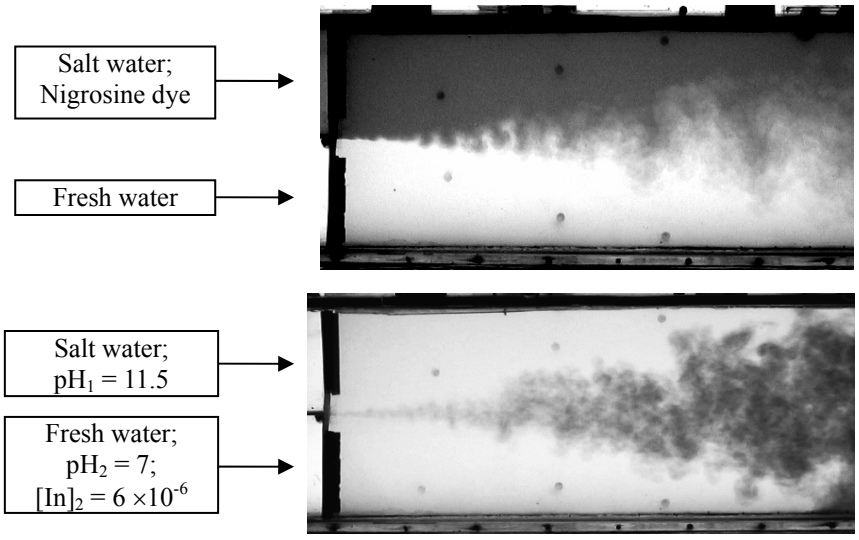

FIGURE 4. Photographs of the buoyancy-generated mixing layer in a typical water channel experiment. In the top photograph (contrast enhanced for visualization), Nigrosine dye was added to the top stream. In the bottom photograph (contrast enhanced for visualization), phenolphthalein was added to the bottom stream, which changes to its pink form as the two streams molecularly mix.

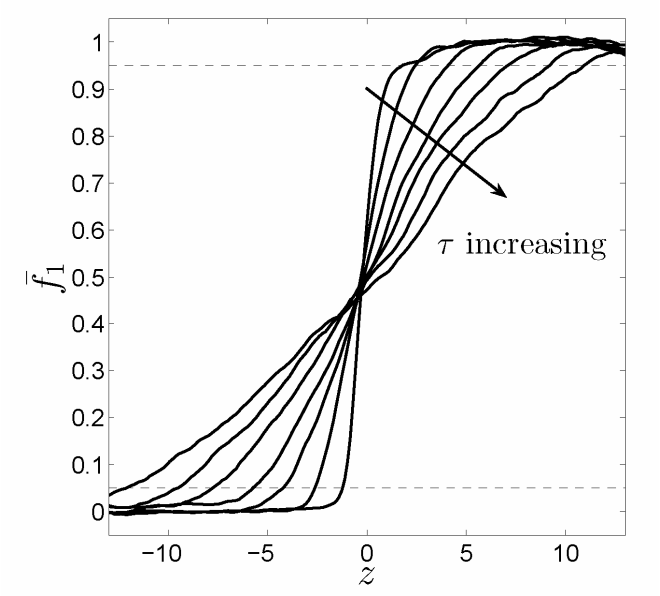

FIGURE 5. Mean volume fraction profiles across the mixing layer at dimensionless times $\tau = 0.25$, 0.50, 0.75, 1.00, 1.25, and 1.50. Fiducials indicating the boundaries of the mixing layer are shown at $\bar{f}_1 = 0.05$ and $\bar{f}_1 = 0.95$.

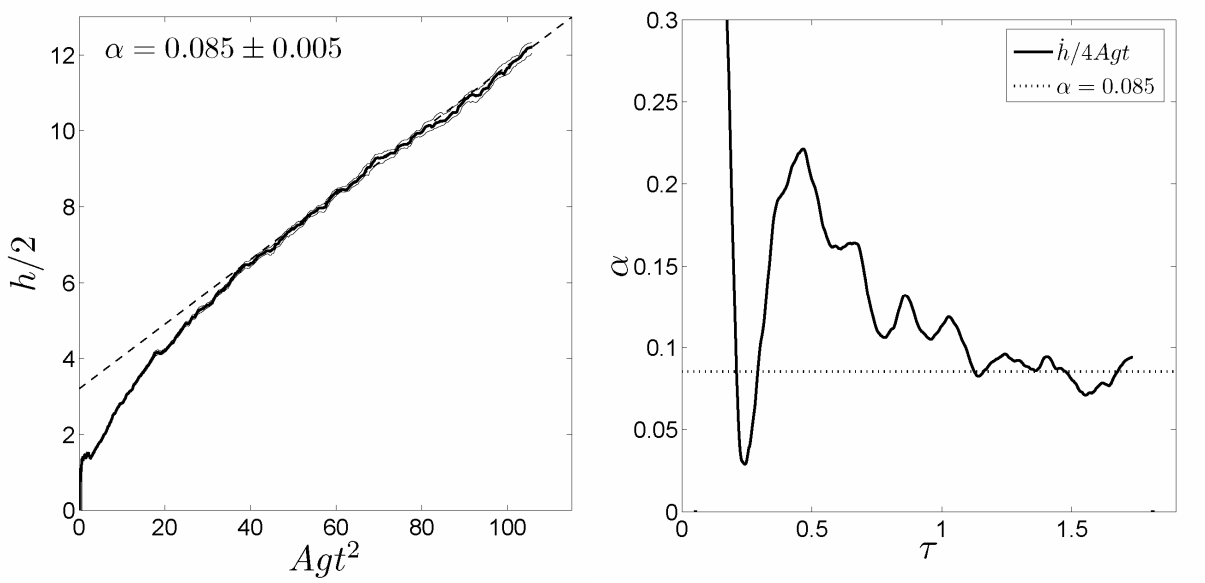

FIGURE 6. Measurement of the mixing layer growth parameter α for the $Sc \sim 10^3$ case. The half-width of the mixing layer is plotted against Agt^2 with 95% confidence interval bounds (left). An alternative measure of α is obtained by normalizing $\dot{h}$ (right). In both figures, a fiducial is shown for $\alpha = 0.085$ (dashed line).

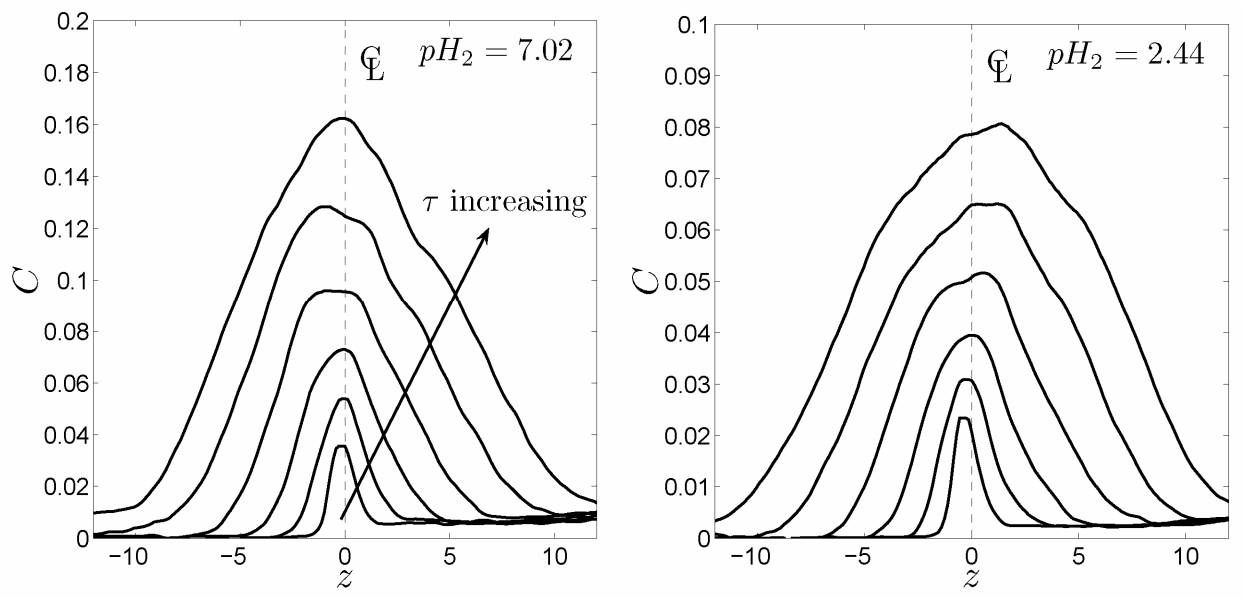

FIGURE 7. Normalized colored indicator concentration profiles across the mixing layer at dimensionless times τ = 0.25, 0.50, 0.75, 1.00, 1.25, and 1.50 for the pH_2 = 7.02 (left) and pH_2 = 2.44 (right) cases, with $pH_1 \approx 11.5$ for both experiments.

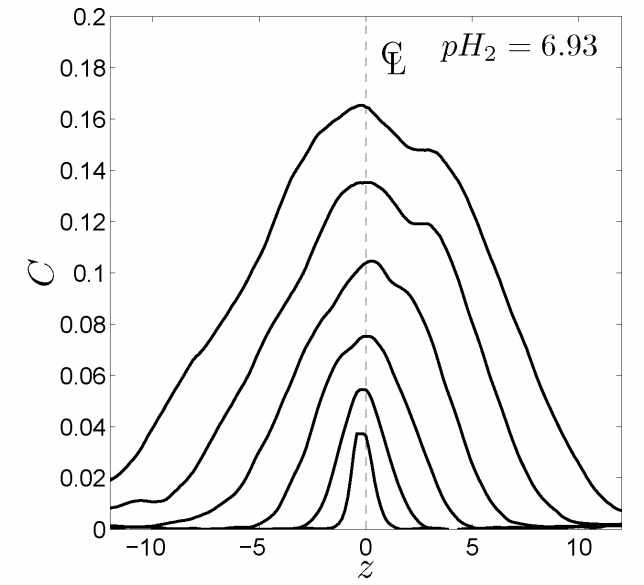

FIGURE 8. Normalized colored indicator concentration profiles across the mixing layer at τ = 0.25, 0.50, 0.75, 1.00, 1.25, and 1.50 for the hot/cold water case.

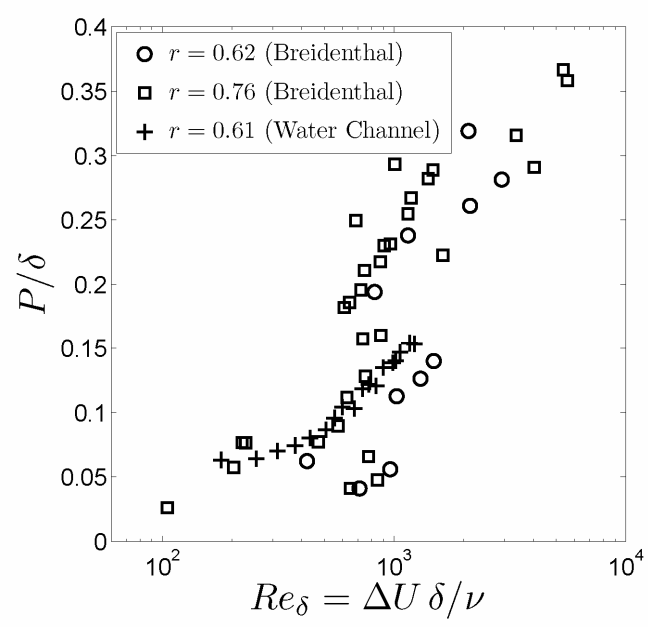

FIGURE 9. Equivalent chemical product thickness, P/δ, for the case of a liquid-phase, turbulent shear layer.

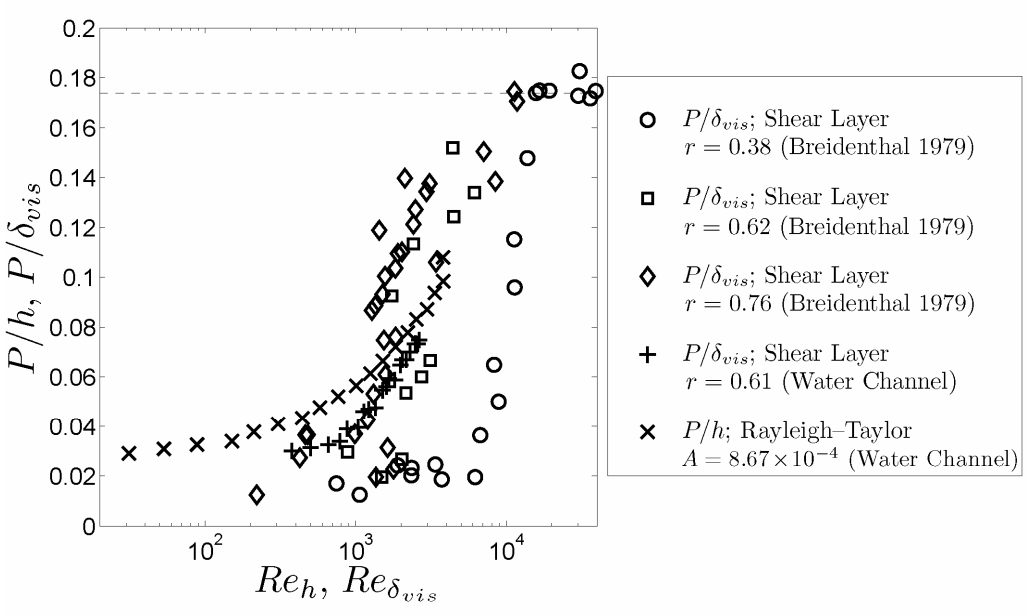

FIGURE 10. Equivalent product thickness for a liquid-phase Rayleigh–Taylor mixing layer, P/h, and shear-driven mixing layers, P/δ_{vis}, at various velocity ratios r. The outer-scale Reynolds numbers are $Re_h = 0.35\sqrt{A\,g\,h^3}\,/\nu$ for the Rayleigh–Taylor case and $Re_{\delta_{vis}} = \Delta U\,\delta_{vis}/\nu$ for the shear case. The asymptotic value $P/\delta_{vis} \approx 0.174$ for shear layers is also shown (dashed line).

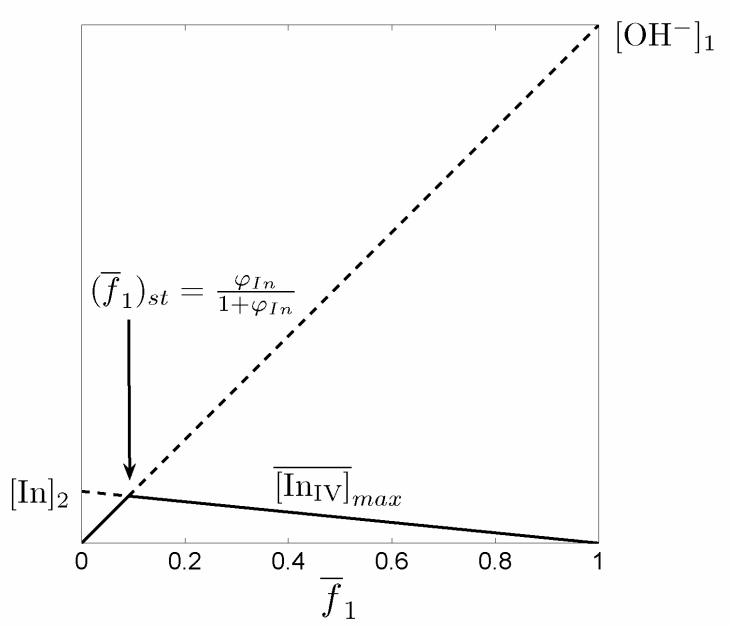

FIGURE 11. Schematic of maximum chemical product formation $\overline{[\mathrm{In_{IV}}]}_{max}$ (solid line) as a function of $\overline{f_1}$ and the equivalence ratio φ_{In}. The peak potential product formation occurs when the stoichiometric ratio of reactants are available at $\left(\overline{f}_1\right)_{st} = \varphi_{\mathrm{In}} / \left(1+\varphi_{\mathrm{In}}\right)$.

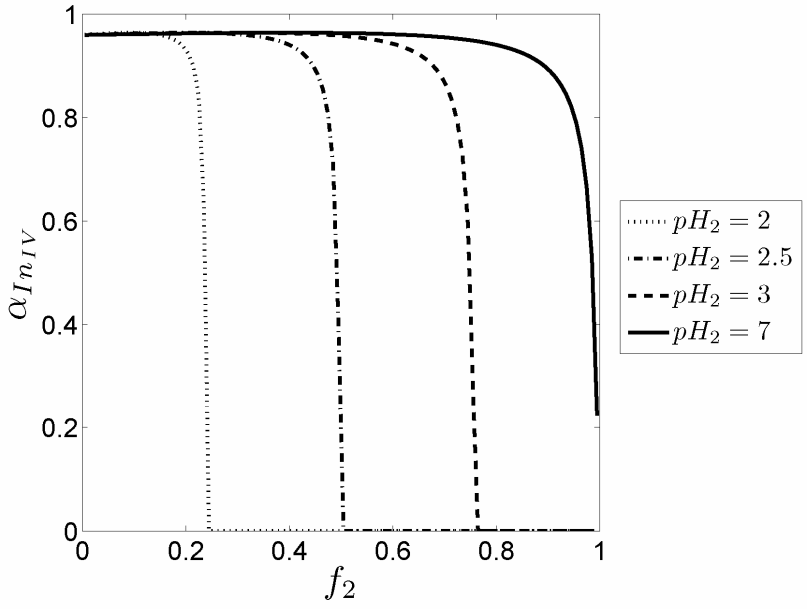

FIGURE 12. Fraction of dissociation for $\mathrm{In_{IV}}$ as a function of the volume fraction f_2 and $\mathrm{pH_2}$ of the acidic stream.

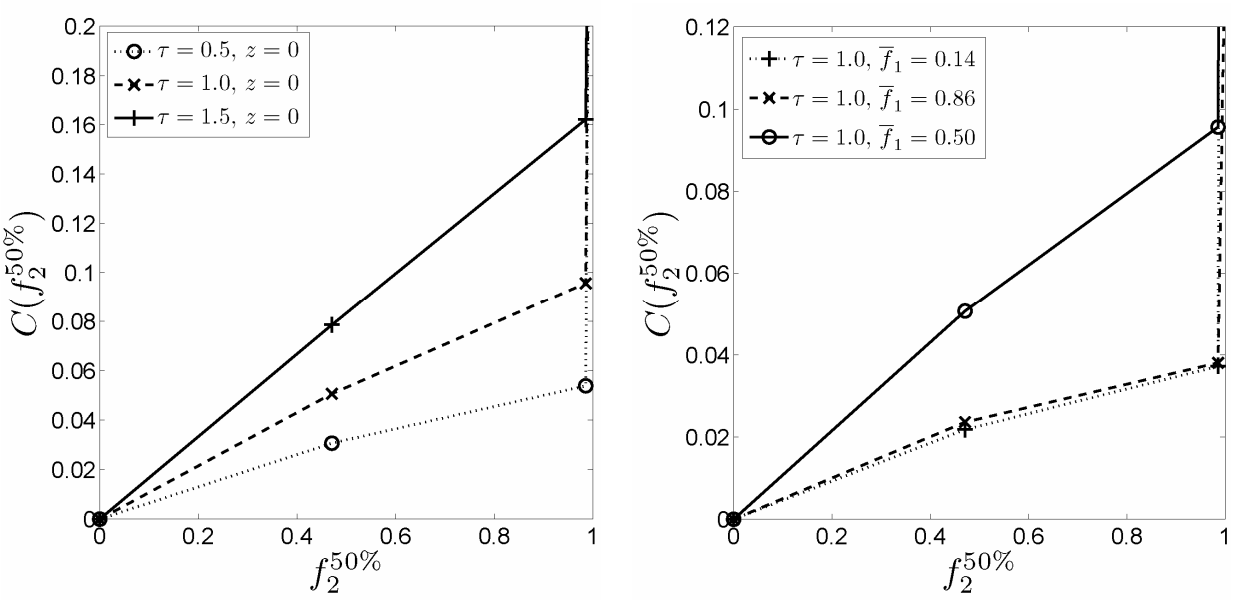

FIGURE 13. Values of colored indicator concentration C for $f_2^{50\%} = 0.471$ (left: pH_1 = 11.52 and pH_2 = 2.44) and $f_2^{50\%} = 0.986$ (right: pH_1 = 11.48 and pH_2 = 7.02) at different downstream locations.

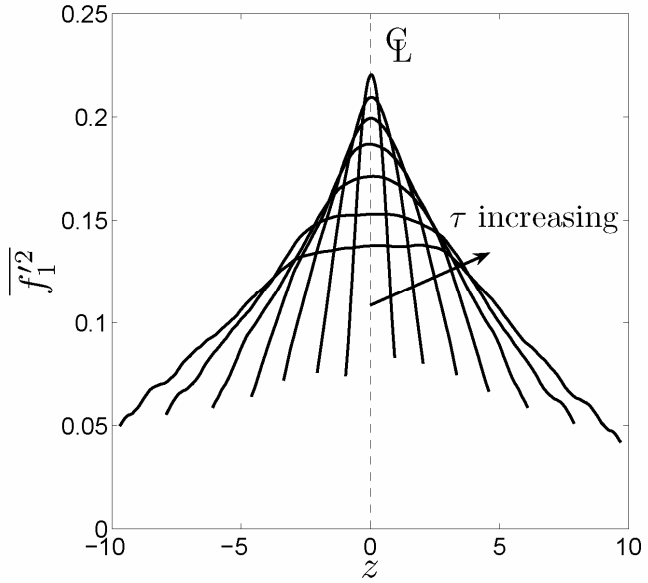

FIGURE 14. Profiles of $\overline{f_1'^2}$ across the mixing layer at dimensionless times $\tau = 0.25$, 0.50, 0.75, 1.00, 1.25, 1.50, and 1.75.

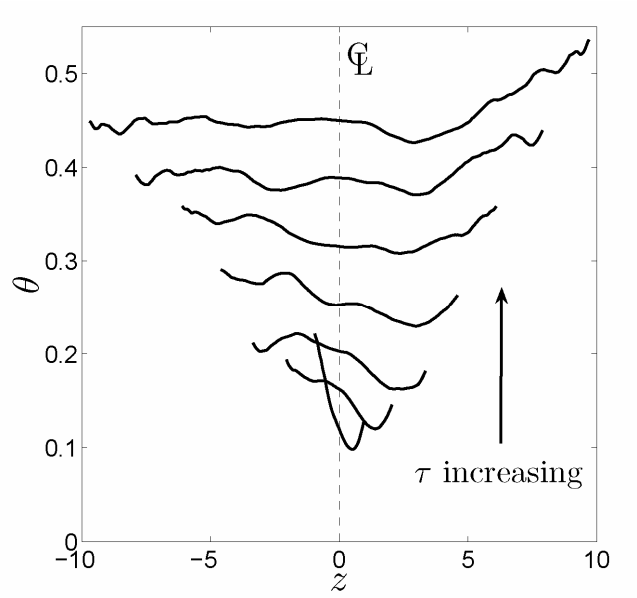

FIGURE 15. Profiles of θ across the mixing layer at dimensionless times $\tau = 0.25$, 0.50, 0.75, 1.00, 1.25, 1.50, and 1.75.

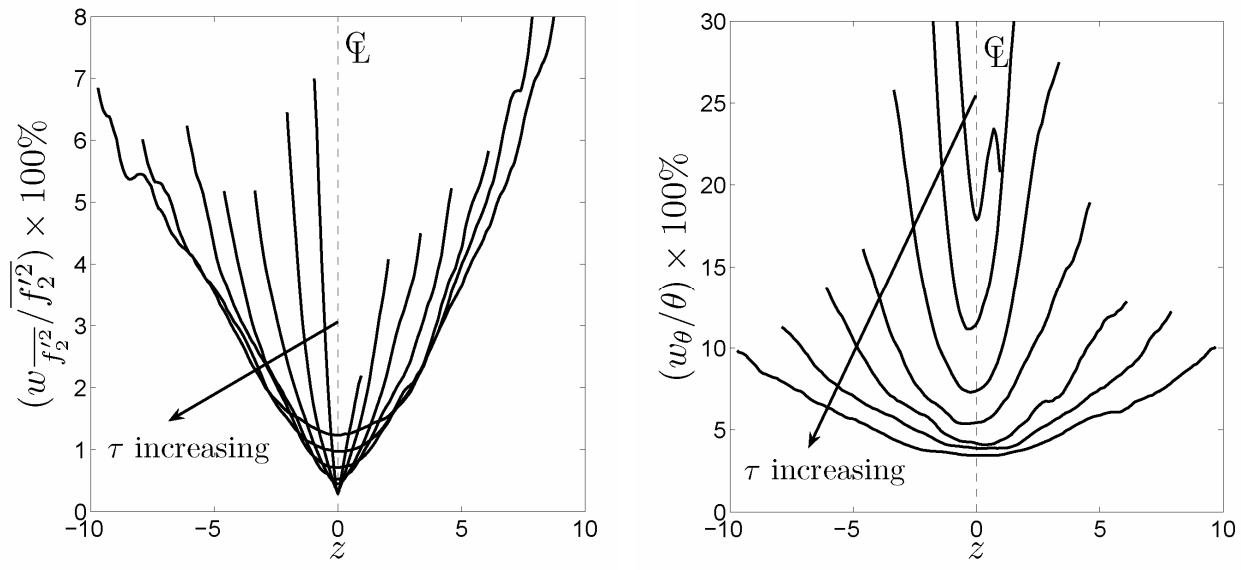

FIGURE 16. Relative uncertainties in the $\overline{f_1'^2}$ (left) and θ (right) profiles at dimensionless times $\tau = 0.25$, 0.50, 0.75, 1.00, 1.25, 1.50, and 1.75.

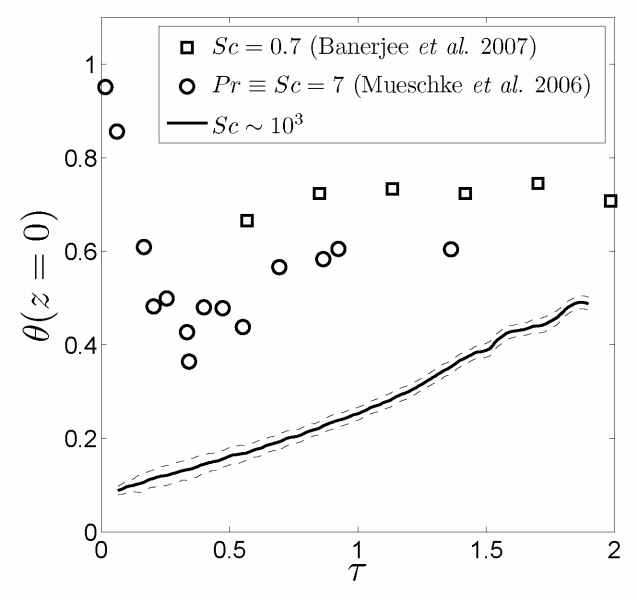

FIGURE 17. Evolution of θ on the centerplane of the mixing layer for various Schmidt numbers. Uncertainty bounds for the $Sc \sim 10^3$ measurements are indicated by the dashed lines. Measurements for the $Sc = 0.7$ case are taken from Banerjee *et al.* (2007), and measurements for $Pr \equiv Sc = 7$ case are taken from Mueschke *et al.* (2006).

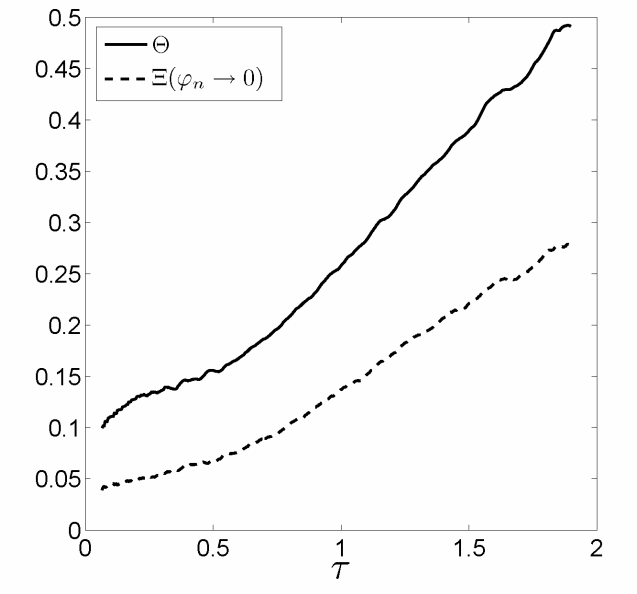

FIGURE 18. Evolution of the global mixing parameters Θ and Ξ for the $Sc \sim 10^3$ case.

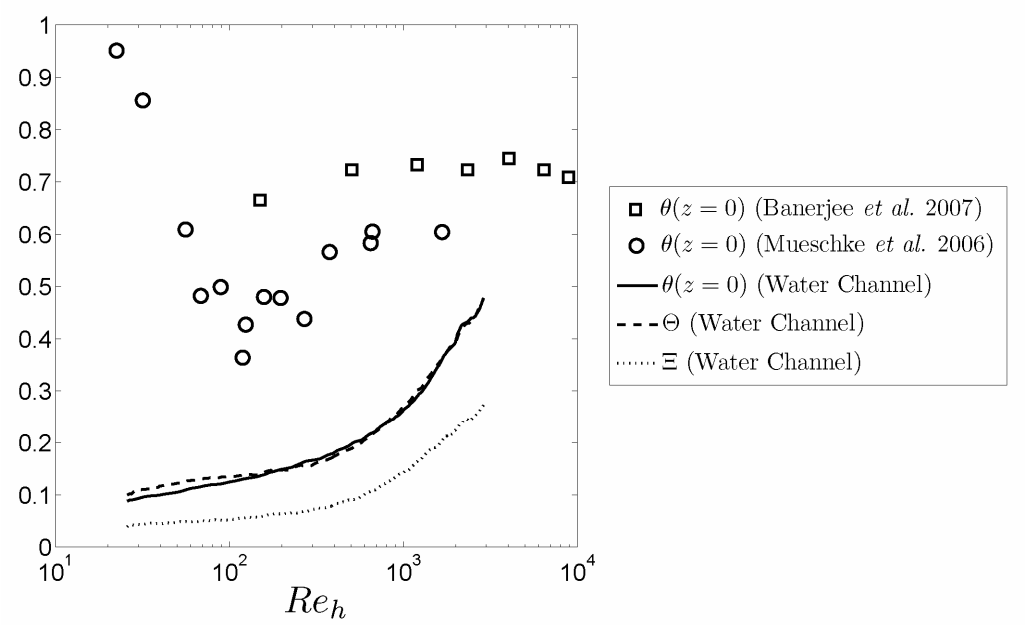

FIGURE 19. Evolution of mixing parameters as a function of Reynolds number $Re_h = 0.35\sqrt{A\,g\,h^3}\,/\nu$.

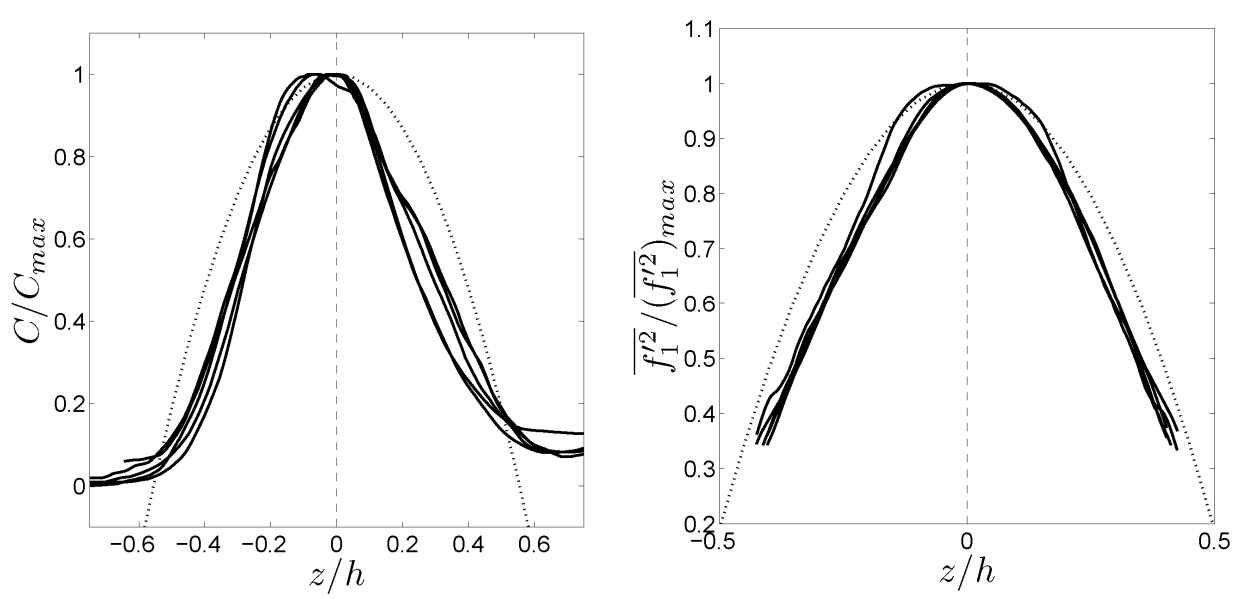

FIGURE 20. Self-similar collapse of the colored indicator concentration (left) and the volume fraction variance (right) profiles. Parabolic profiles are shown as a reference (dotted line).